

1 Influence of Ocean Alkalinity Enhancement with Olivine or Steel 2 Slag on a Coastal Plankton Community in Tasmania

3
4 Jiaying A. Guo^{1,2}, Robert F. Strzepek², Kerrie M. Swadling^{1,2}, Ashley T. Townsend³, Lennart T. Bach¹

5 ¹Institute for Marine and Antarctic Studies, University of Tasmania, Hobart, Tasmania, 7000 Australia

6 ²Australian Antarctic Program Partnership (AAPP), Institute for Marine and Antarctic Studies, University of Tasmania,
7 Hobart, Tasmania, 7000 Australia

8 ³Central Science Laboratory, University of Tasmania, Sandy Bay, Tasmania, 7005 Australia

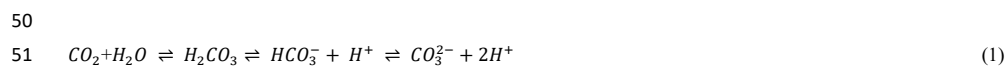
9 Correspondence to: Jiaying A. Guo (Jiaying.guo@utas.edu.au)

10
11 **Abstract.** Ocean alkalinity enhancement (OAE) aims to increase atmospheric CO₂ sequestration in the oceans through the
12 acceleration of chemical rock weathering. This could be achieved by grinding rocks containing alkaline minerals and
13 adding the rock powder to the surface ocean where it dissolves and chemically locks CO₂ in seawater as bicarbonate.
14 However, CO₂ sequestration during dissolution coincides with the release of potentially bio-active chemicals and may
15 induce side effects. Here, we used 53 L microcosms to test how coastal plankton communities from Tasmania respond to
16 OAE with olivine (mainly Mg₂SiO₄) or steel slag (mainly CaO and Ca(OH)₂) as alkalinity sources. Three microcosms were
17 left unperturbed and served as a control, three were enriched with olivine powder (1.9 g L⁻¹), and three with steel slag
18 powder (0.038 g L⁻¹). Olivine and steel slag powders were of similar grain size. Olivine was added in a higher amount than
19 the steel slag with the aim to compensate for the lower efficiency of olivine to deliver alkalinity over the 3-week experiment.
20 Phytoplankton and zooplankton community responses as well as some biogeochemical parameters were monitored. Olivine
21 and steel slag additions increased total alkalinity by 29 μmol kg⁻¹ and 361 μmol kg⁻¹ respectively, which corresponds to a
22 theoretical increase of 0.9 % and 14.8 % of the seawater storage capacity for atmospheric CO₂. Olivine and steel slag
23 released silicate nutrients into the seawater, but steel slag released considerably more and also significant amounts of
24 phosphate. After 21 days, no significant difference was found in dissolved iron concentrations (>100 nmol L⁻¹) in the
25 treatments and the control. The slag addition increased dissolved manganese concentrations (771 nmol L⁻¹), while olivine
26 increased dissolved nickel concentrations (37 nmol L⁻¹). There was no significant difference in total chlorophyll *a*
27 concentrations between the treatments and the control, likely due to nitrogen limitation of the phytoplankton community.
28 However, flow cytometry results indicated an increase in the cellular abundance of several smaller (<20 μm)
29 phytoplankton groups in the olivine treatment. The abundance of larger phytoplankton (>20 μm) decreased much more
30 in the control than in the treatments after day 10. Furthermore, the maximum quantum yields of photosystem II (F_v/F_m)
31 were higher in slag and olivine treatments, suggesting that mineral additions increased photosynthetic performance. The
32 zooplankton community composition was also affected with the most notable changes being observed in the dinoflagellate
33 *Noctiluca scintillans* and the appendicularian *Oikopleura* sp. in the olivine treatment. Overall, steel slag is much more
34 efficient for CO₂ removal with OAE than olivine and appears to induce less change in the plankton community when
35 relating the CO₂ removal potential to the level of environmental impact that was observed here.

36 1 Introduction

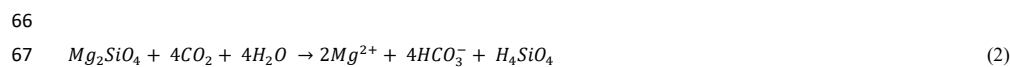
37 Keeping global warming below 2 °C requires immediate emissions reduction. Additionally, between 450-1100 Gigatonnes
38 of carbon dioxide (CO₂) need to be removed from the atmosphere by 2100 (Smith et al., 2023). This could be achieved
39 with a portfolio of terrestrial and marine Carbon Dioxide Removal (CDR) methods. Ocean alkalinity enhancement (OAE)
40 is a marine CDR method that could theoretically contribute significantly to the global CDR portfolio (Ilyina et al., 2013;
41 Feng et al., 2017; Lenton et al., 2018).

42
43 Alkalinity is generated naturally when rock weathers and it has control on the ocean's chemical capacity to store CO₂
44 (Schuiling and Krijgsman, 2006). Natural rock weathering is currently responsible for about 0.5 Gt of atmospheric CO₂
45 sequestration every year (Renforth and Henderson, 2017). The idea behind OAE is to accelerate natural rock weathering
46 by extracting calcium- or magnesium-rich rocks, such as olivine, pulverizing them, and spreading them onto the sea surface
47 to increase chemical weathering rates (Hartmann et al., 2013). The weathering (i.e., dissolution) of these alkaline minerals
48 will consume protons (H⁺), which shifts the carbonate chemistry equilibrium in seawater from CO₂ towards increasing
49 bicarbonate (HCO₃⁻) and carbonate ion (CO₃²⁻) concentrations:



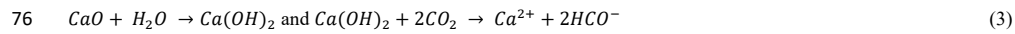
52
53 thereby making new space for atmospheric CO₂ to be dissolved in seawater and permanently stored. Previous model studies
54 have shown that OAE can mitigate climate change significantly by increasing the oceanic uptake of CO₂ from the
55 atmosphere (Kohler et al., 2010; Paquay and Zeebe, 2013; Keller et al., 2014; Lenton et al., 2018). For example, the study
56 by Burt et al. (2021) suggested that the total global mean dissolved inorganic carbon (DIC) inventories would increase by
57 156 GtC after total alkalinity is enhanced at a rate of 0.25 Pmol year⁻¹ in 75-year simulations.

58
59 There are a variety of alkaline minerals that could be used for OAE. A widely considered naturally occurring mineral is
60 forsterite, a (Mg₂SiO₄)-rich olivine. This type of olivine is abundant in ultramafic rock such as dunite, constituting at least
61 88 % of the rock composition (Ackerman et al., 2009; Su et al., 2016). Olivine occurs in the Earth's crust but is more
62 abundant in the upper mantle. There are at least several billion tons of olivine resources on Earth (Caserini et al., 2022).
63 However, the extraction of olivine in 2017 was only around 8.4 Mt year⁻¹ (Reichl et al., 2018), which is about two orders
64 of magnitude below the mass needed for climate-relevant OAE with olivine (Caserini et al., 2022). The net reaction for
65 CO₂ sequestration with Mg₂SiO₄ is:



68
69 Another potential OAE source material is steel slag (Renforth, 2019), a by-product of steel manufacturing. During steel
70 manufacturing, high-purity calcium oxide (CaO) is used to improve the quality of the steel through accumulation of
71 unwanted materials such as sulphur and phosphorus. Steel slag mainly contains CaO, SiO₂, Al₂O₃, Fe₂O₃, MgO, and MnO
72 (Kourounis et al., 2007), and the chemical composition can vary depending on the manufacturing process (Wang et al.,
73 2011). Due to the presence of CaO and potentially other alkaline components, steel slag can increase alkalinity when
74 dissolved in seawater. The chemical reaction for CO₂ sequestration with CaO is:

75



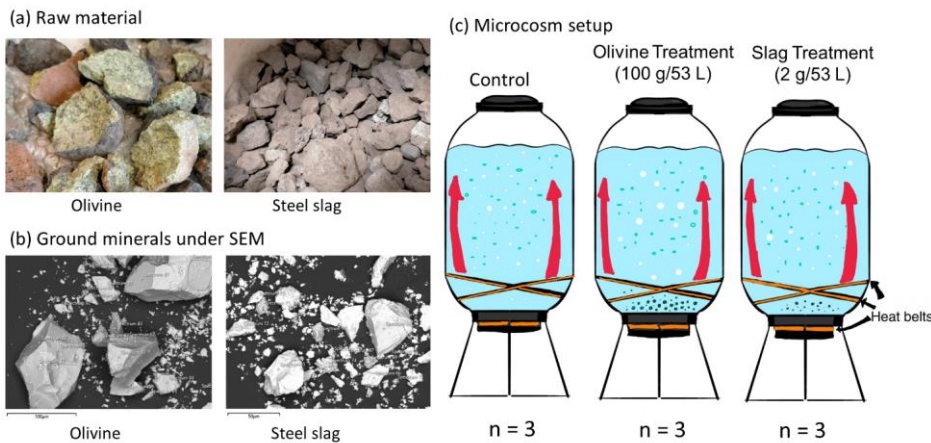
78 Some of the steel slag that is produced during steel manufacturing is further used (e.g., for road construction and civil
79 engineering) but in some countries like China, 70.5 % of steel slag is left unused and stored in dumps (Guo et al., 2018).
80 In 2016, more than 300 million tons of steel slag was not used effectively, thereby occupying the land and raising
81 environmental concerns (Guo et al., 2018). The effective alkaline composition, availability, and relatively low cost of the
82 raw materials make olivine and steel slag potential source materials for OAE.
83

84 To assess whether OAE is viable, it needs to be understood how its application may affect marine biota such as plankton
85 and the biogeochemical fluxes they drive. Some data on the effects of OAE with sodium hydroxide (NaOH) on plankton
86 communities have recently been published (Ferderer et al., 2022; Subhas et al., 2022), but to the best of our knowledge, no
87 such data are available for olivine- and/or slag-based OAE. Chemical perturbations via olivine and slag should be like
88 those by NaOH in that they increase seawater pH and shift the carbonate chemistry equilibrium (see Eq. 1). However, there
89 would be additional chemical perturbations because minerals contain a variety of potentially bioactive elements that are
90 released into the environment when they dissolve in seawater (Bach et al., 2019). One particular concern is that natural and
91 anthropogenic minerals such as olivine and steel slag are rich in bioactive metals that are usually scarce in the ocean, such
92 as iron (Fe), copper (Cu), nickel (Ni), manganese (Mn), zinc (Zn), cadmium (Cd), and chromium (Cr). Many of these trace
93 metals are essential micronutrients for phytoplankton growth (Sunda, 2000; Sunda, 2012), such as being co-factors for
94 various metalloenzymes (summarized by Twining and Baines, 2013). It is possible that the addition of alkaline minerals
95 may benefit phytoplankton by providing trace metals currently limiting phytoplankton growth (Falkowski, 1994; Basu and
96 Mackey, 2018). For instance, the addition of Fe is well known to stimulate phytoplankton blooms in those vast ocean
97 regions where Fe levels limit growth (Boyd et al., 2007; Moore et al., 2013). However, some trace metals can also inhibit
98 phytoplankton growth, and different phytoplankton species have different requirements and tolerances for trace metals
99 (Sunda, 2012) so the addition of trace metals via OAE may change phytoplankton community composition.
100

101 Here, we describe a microcosm experiment with coastal Tasmanian plankton communities that was used to investigate: (1)
102 how effectively OAE via the application of finely ground olivine and steel slag could sequester atmospheric CO₂, and (2)
103 if/how olivine and steel slag additions affect various components of the plankton community.
104

105 **2 Methodology**

106 **2.1 Microcosm setup**



107
108 **Fig. 1.** Experimental design and alkalinity sources. (a) Raw materials used as alkalinity sources: olivine (left) and steel slag (right).
109 Olivine and steel slag were originally larger than 20 mm. (b) Ground minerals observed with a scanning electron microscope (SEM). (c)
110 Microcosm setup: each microcosm enclosed ~ 53 L of surface seawater with natural plankton communities. Olivine and steel slag
111 treatments and the control were kept in a temperature-controlled room and two heat belts were attached to the bottom of each microcosm
112 to create convective circulation.

113
114 We used nine 53 L transparent Kegland® Fermzilla conical unitank fermenters (polyethylene terephthalate) (Fig. 1) as
115 microcosms to incubate natural plankton communities. All microcosms were prewashed with hydrochloric acid (10 % v/v)
116 and rinsed five times with 18.2 MΩ Milli-Q water. Seawater with coastal plankton communities was collected at Battery
117 Point, Tasmania (42.892°S, 147.337°E) within 2 hours by lowering the microcosms into the ocean with a crane and filling
118 them in a manner similar to a Niskin bottle, as described in detail in Ferderer et al. (2022). A sieve with a mesh size of 2
119 mm was attached to the top and bottom of the microcosms during filling to avoid the entrapment of large and patchily
120 distributed organisms in the microcosms. The enclosed seawater weight was initially between 52.35-54.70 kg. After
121 seawater collection, filled microcosms were immediately transported back to the Institute for Marine and Antarctic Studies
122 (University of Tasmania) on a truck and transferred within 75 min into a temperature-controlled room set to 7.5-8 °C. Two
123 heat belts were attached to the bottom of each microcosm to induce a convective mixing current (Ferderer et al., 2022).
124 Seawater temperature inside the microcosms was about 13.5 °C due to the heating effects of the heat belts and was the
125 same as the sampled region. LED light strips were used to provide an average light intensity of 236 $\mu\text{mol photons m}^{-2} \text{s}^{-1}$
126 (ranging from 208 to 267 $\mu\text{mol photons m}^{-2} \text{s}^{-1}$) with a daily light-dark cycle of 10:14 hours. The light intensity was the
127 average light intensity in each microcosm measured with a LICOR light meter at 0.15 m depth within the microcosm.
128 Microcosms positioned in the temperature-controlled room were shuffled anti-clockwise every day to ensure similar light

129 intensity for each microcosm throughout the experiment. Treatments were established 24 hours after collecting the seawater.
130 The total alkalinity released per amount of mineral powder added was much higher for the slag powder than the olivine
131 powder in our preliminary test trials. So, three microcosms were enriched with 100 g of olivine powder, three microcosms
132 with 2 g of steel slag powder, while the remaining three microcosms were left unperturbed and served as controls.

133
134

135 **2.2 Preparation of olivine and steel slag powder**

136 The olivine rocks were provided by Moyne Shire Council who sourced the mineral from a quarry in Mortlake, Victoria,
137 Australia. The Basic Oxygen Slag (hereafter referred to as “slag”) was provided by Bradley Mansell who sourced the
138 material from Liberty Primary Steel Whyalla Steelworks in Whyalla, South Australia, Australia. Upon delivery, the olivine
139 rocks were 40-80 mm in diameter, and slag aggregates were 20-50 mm in diameter. These were crushed to smaller than 10
140 mm pieces using a hydraulic crusher. The crushed material was further ground with a ring mill with a chrome milling pot.
141 Afterwards, finely-ground samples were sieved to get samples with 150 ~ 250 μm grain size. The sieved olivine and slag
142 grains were inspected for their appearance and elemental composition using a Hitachi SU-70 analytical field emission
143 scanning electron microscope (SEM), and energy dispersive spectrometers (Central Science Laboratory (CSL), University
144 of Tasmania). Grain size spectra were determined with a Sympatec QICPIC particle size analyser LIXCELL (CSL,
145 University of Tasmania).

146

147 **2.3 Seawater sampling**

148 Seawater was transferred with a peristaltic pump from the microcosms at a depth of about 0.15 m into 1 L acid-washed
149 sampling bottles (LDPE) using an acid-washed silicon tube. Seawater in these bottles was then subsampled for dissolved
150 trace metal samples, filtrations, Fast Repetition Rate fluorometry (FRRF), and flow cytometry analysis. Samples for
151 nutrients and total alkalinity (TA) were transferred using the same pump but through a silicone tube into 80 mL HDPE
152 bottles. Total alkalinity and macronutrient samples were filtered during this process through a 0.2 μm nylon filter attached
153 to the silicone tube to remove all particles and organisms $> 0.2 \mu\text{m}$.

154

155 **2.4 Salinity, nutrients, carbonate chemistry, and trace metal analysis**

156 Salinity was measured before and at the end of the experiment using a HACH HQ40d portable meter. The pH_T (total scale)
157 and temperatures were measured daily (2-3 hours after the onset of the light period) using a pH meter (914
158 pH/Conductometer Metrohm). We recorded voltages and temperature from the pH meter and calibrated the pH_T at original
159 temperature at sampled time using the certified reference material (CRM) Tris buffer following the method described in
160 SOP6a by Dickson et al. (2007). Briefly, the standard buffer's pH and voltage at different temperature gradients were
161 recorded, and temperature vs. voltage polynomial regression data were generated for calculating calibrated pH values (pH_T)
162 (refer to Eq. 3 in SOP6a of Dickson et al. (2007)). The regression could then be used to obtain a CRM pH value for each
163 temperature and to calibrate the pH measured in the microcosms to the total pH scale.

164

165 Total alkalinity was sampled every four days. It was measured in duplicate using a Metrohm 862 Compact Titrosampler
166 coupled with an Aquatrode Plus with PT1000 temperature sensor following the SOP3b open-cell titration protocol
167 described in Dickson et al. (2007). Filtered TA samples were stored at 8 °C for a maximum of 23 days before measurement.
168 Titration curves were evaluated using the “calculate” script within PyCO2sys by Humphreys et al. (2022). The carbon
169 chemistry equilibrium was calculated with the R package “seacarb” Gattuso et al. (2023) from pH_T , TA, phosphate, silicate,
170 temperature, and salinities using stoichiometric equilibrium constants from Lueker et al. (2000). Dissolved macronutrients
171 were measured every second day using standard spectrophotometric methods developed by Hansen and Koroleff (1999)
172 on the day the samples were taken from the microcosms.

173

174 Dissolved trace metal concentrations were measured four times during the experiment: a few hours before olivine and slag
175 were added, a few hours after these minerals were added on day 2, near the middle of the experiment on day 13, and at the
176 end of the experiment on day 22. Sixty mL of seawater was collected using an acid-washed 60 mL syringe, and the seawater
177 was filtered through 25 mm diameter 0.2 µm pore size polycarbonate filters. Unfortunately, we did not notice that 0.2 µm
178 pore size nylon filters (acid washed) were used during sampling on days 1 and 2 so we refiltered these seawater samples
179 again using 0.2 µm pore size polycarbonate filters after one month. All seawater samples were diluted approximately 20-
180 fold by weight using Milli-Q water (18.2 MΩ·cm grade) and acidified using 1 % ultrapure HCl. These samples were
181 analysed using Sector Field Inductively Coupled Plasma Mass Spectrometry (SF-ICP-MS) employing multiple resolution
182 settings to overcome major spectral interferences. Due to the presence of abundant major metal ions in our samples, such
183 as Na and Mg, natural open-ocean seawater from the Southern Ocean with very low trace metal concentrations was diluted
184 20 times with Milli-Q water and used as a representative blank. The same Southern Ocean seawater was enriched with
185 different gradients of trace metal standards to calculate the samples’ trace metal concentrations. Five of the total 36 samples
186 had abnormal trace metal concentrations, and 2 of them were from day 1. We considered values as outliers using the
187 interquartile range (IQR) criterion on pre-addition data, and if values are more than 10 times higher than replicates, they
188 are also considered as outliers. These samples containing outliers were excluded from the data analysis (Table S1.). The
189 major likely source of these metal contaminations is sampling in the temperature control room, where precautions were
190 insufficiently implemented.

191

192 **2.5 Particulate matter and plankton community analysis**

193 Chlorophyll *a* was sampled every second day by filtering the seawater through glass fibre filters (GF/F, pore size = 0.7 µm,
194 diameter = 25 mm), and filters were stored in 15 mL polypropylene tubes wrapped with aluminium foil and stored at -80 °C
195 for 50-70 days before measurement. Each filter was immersed in 10 mL 100 % methanol for 18-20 h to extract chlorophyll
196 from phytoplankton and these samples were analysed on a Turner fluorometer (Model 10-AU) following the method
197 described by Evans et al. (1987).

198

199 Phytoplankton flow cytometry samples were fixed with 40 µL of a mixture of formaldehyde-hexamine (18 %:10 % v/w)
200 added to 1400 µL of seawater sample. All bacteria samples (700 µL) were fixed with 14 µL glutaraldehyde (Electron-
201 microscope grade, 25 %). After mixing samples with fixatives, samples were stored for 25 minutes at 10 °C, then flash-
202 frozen in liquid nitrogen, and stored at -80 °C until measurement 83-86 days later. Directly before the measurement,
203 samples were thawed at 37 °C. Bacteria samples were stained with SYBR green I (diluted in dimethylsulfoxide) at a final

204 ratio of 1:10000 (SYBR Green I: sample).

205

206 A Cytex Aurora flow cytometer (Cytex Biosciences) was used to quantify the abundance of fluorescing particles such as
207 phytoplankton or stained bacteria. Phytoplankton groups were distinguished based on their fluorescence signal intensity of
208 different laser excitation/emission wavelength combinations and forward scatter (FSC). The yellow-green laser (centre
209 wavelength: 577 nm), in combination with FSC signal strength, was used to separate cyanobacteria and cryptophytes from
210 other phytoplankton. The violet laser (centre wavelength: 664 nm) in combination with FSC was used to distinguish
211 picoeukaryotes, nanoeukaryotes, and microphytoplankton. The blue laser (centre wavelength: 508 nm) in combination with
212 FSC was used to distinguish bacteria from other living (i.e., DNA-containing) particles (Fig. S. 1).

213

214 The biovolume of each classified flow cytometry phytoplankton type was calculated using the equation:

215

$$216 \text{ Biovolume} = \text{Cell number count} \times \left(\frac{\text{FSC}}{10248}\right)^{2.14} \quad (4)$$

217

218 where biovolume is the biovolume of the phytoplankton (μm^3), cell number is the cell count per mL of sample, and the
219 FSC is the forward scatter signal value from the flow cytometry. This equation is calculated based on the relationship
220 between biovolume and FSC for different phytoplankton species (Selfe, 2022). The biovolume of each phytoplankton type
221 was then divided by the total biovolume of all phytoplankton type to calculate the biovolume proportion of each
222 phytoplankton type (Biovolume prop.). This derived value was used to estimate the phytoplankton composition in each
223 microcosm.

224

225 Phytoplankton photosynthetic performance was estimated from the rapid light curves measured with an FRRf (FastOcean
226 Sensor FRRf3, Chelsea Instruments Group) every second day following the protocol adapted from Schallenberg et al.
227 (2020). Samples were kept in the dark for 20 minutes before the measurement and then added to the FRR fluorometry
228 cuvette, which was temperature-controlled at 13.5 °C. Filtered natural seawater was used for blank correction. A channel
229 with three light wavelengths (450, 530, and 624 nm) was used in each acquisition sequence. At least 10 acquisitions were
230 measured for each sample. The maximum electron transport rate (ETR_{max}), initial slope of the rapid light curve (α), and the
231 light-saturation parameter (E_k) were calculated using the equation described by Platt et al. (1980) without photoinhibition:

232

$$233 \text{ ETR} = \text{ETR}_{\text{max}} \left[1 - e^{-\frac{\alpha E}{\text{ETR}_{\text{max}}}}\right] \quad (5)$$

234

235 These parameters together with the maximum quantum yield of PSII (F_v/F_m) were used to compare the photosynthetic
236 performance of the phytoplankton communities in different microcosms.

237

238 Seawater was sampled before the treatment and at the end of the experiment for particulate trace metal concentrations.
239 Samples of 100 mL were filtered through an acid-cleaned polycarbonate filter (25 mm diameter, 0.8 μm pore size) and
240 placed in an acid-cleaned polypropylene filter holder in a trace metal-clean laminar flow bench. The filters were washed
241 with the EDTA-oxalate reagent (1.4 mL) twice (8 min total) and rinsed with chelexed NaCl solution (0.6 mol L^{-1} with 2.38
242 mmol L^{-1} of HCO_3^- , pH=8.2) 10 times (1.5 mL aliquots) (Tovar-Sanchez et al., 2003; Tang and Morel, 2006). Filters were
243 stored in acid-washed well plates at -20 °C before analysis. The digestion process followed the method reported by Bowie

244 et al. (2010). Briefly, all samples and triplicate certified reference materials plankton standards (50 mg/vial) were digested
245 in a mixture of strong ultrapure acids (750 μL 12 mol L^{-1} HCl, 250 μL 40 % HF, 250 μL 14 mol L^{-1} HNO_3) in 15 mL Teflon
246 perfluoroalkoxy (PFA) vials on a 95 $^\circ\text{C}$ hot plate for 12 h in a fume hood. They were then dry evaporated for 4 h and re-
247 suspended in 10 % v-v ultrapure HNO_3 . All prepared solutions had indium as internal standard added to a final
248 concentration of 10 μg L^{-1} . Three pre-mixed multi-element standard solutions (MISA) were prepared as external calibration
249 standards.

250
251 Particulate organic carbon (POC) was sampled by filtering 100 mL of seawater from each microcosm. Glass fibre filters
252 (Whatman GF/F, pore size = 0.7 μm , diameter = 13 mm) were pre-combusted at 400 $^\circ\text{C}$ for 6 h. Filters were stored at -20 $^\circ\text{C}$
253 before measurement. Samples were treated via fuming with 2N HCl to remove carbonates overnight and dried in the oven
254 for 4h. Finally, filters were folded into silver cups and stored in a desiccator until analysis. Samples were analysed for
255 carbon with a Thermo Finnigan EA 1112 Series Flash Elemental Analyser (CSL, University of Tasmania).

256
257 Biogenic silica (BSi) concentrations were analysed every 4 days by filtering 100 mL of seawater from each microcosm.
258 Mixed Cellulose Ester (MCE) membrane filters (diameter = 25 mm, pore size = 0.8 μm) were used for BSi samples. BSi
259 filters were placed in a plastic petri dish and stored at -20 $^\circ\text{C}$ before measurement. Filters were processed using the hot
260 NaOH digestion method of Nelson et al. (1989). The final solution was measured using the same process as the dissolved
261 silicate (see section 2.4).

262
263 A self-made plastic zooplankton net (20 mm height and 15 mm width) with a 210 μm mesh size was acid-washed first and
264 then used to collect zooplankton from microcosms before mineral addition on day 2, near the middle (day 13), and at the
265 end of the experiment (day 23). Samples were stored in 10 % formalin seawater solutions and kept at room temperature
266 until measurements. Zooplankton were quantified and identified under a Leica M165C microscope fitted with a Canon 5D
267 camera. The number of zooplankton from one mini-trawl in each collection was converted to the unit of individual L^{-1} and
268 used for data analysis. The diversity of zooplankton communities was estimated with the Shannon Diversity Index (H)
269 calculated as:

$$270 \quad H = -\sum(p_i \times \ln(p_i)) \quad (6)$$

271
272 where p_i is the proportion of the entire zooplankton community made up of individual species abundance, and \ln is the
273 natural logarithm.
274

275
276

277 **2.6 Statistic analysis**

278 R studio was used for data analyses. Generalized additive models (GAMs) from the package “mgcv” were fitted to the data
279 to predict the changes over time. The GAMs all shared the same equations:

$$280 \quad Y = s(\text{Day}), \quad (7)$$

282

283 in which Y presents the dependent variable and $s(\text{Day})$ is the smooth term of the day of the experiment. Another GAM was
284 used to detect significant differences between treatments and the control:

$$285 \quad Y = \textit{Treatment} + s(\textit{Day}) + s(\textit{Day}, \textit{by} = \textit{oTreatment}) \quad (8)$$

287
288 In this equation, the variable “Treatment” includes three conditions: “Control”, “Slag” and “Olivine”; while “oTreatment”
289 is the ordered factor of the variable “Treatment” which allowed us to compare the GAMs smooth terms from different
290 treatments and the control (Simpson, 2017).

291
292 When comparing GAMs, P-means represent the p-value obtained from comparing two GAMs, such as the control and the
293 olivine treatment. If P-means is below 0.05, it indicates that the mean values of the two GAMs exhibit significant
294 differences over the course of the experiment. Conversely, if P-means is equal to or greater than 0.05, it suggests that the
295 two GAMs have similar mean values. In contrast, P-smooths represents the p-value derived from comparing the smooth
296 terms of two GAMs. If P-smooths is below 0.05, it indicates that the two GAMs demonstrate significantly different trends
297 in their change over time.

298
299 For the analysis of trace metal concentrations and zooplankton abundance, Generalized Linear Models (GLMs) from the
300 'stats' package were fitted to the data to determine significant differences between treatments and the control. The selection
301 of specific GLMs was based on the distribution of the raw data. One GLM equation is

$$302 \quad Y = \textit{Treatment} + \frac{\textit{Day}}{22} + \left(\frac{\textit{Day}}{22}\right)^2 \quad (9)$$

304
305 with family = Gamma, where Y represents the measured parameter (abundance of a zooplankton species and dissolved
306 trace metal concentrations); treatment is the conditions (“Control”, “Slag” and “Olivine”); and Day represents the day of
307 the experiment. The other GLM equation,

$$308 \quad Y = \textit{Treatment} + \textit{Day} \quad (10)$$

310
311 with family = Gaussian, was employed for particulate trace metal data and the Shannon Diversity Index. To compare the
312 contribution of the three treatments on the measured parameters, Tukey's significant difference test was conducted on the
313 GLMs using the 'glht' function.

314

315 **3. Results**

316 **3.1 Elemental composition and grain size of the finely-ground minerals**

317 SEM analysis revealed the approximate elemental composition of olivine and slag powder (Table 1). Based on this analysis
318 the olivine composition resembles the Mg-rich olivine mineral “forsterite” (Mg_2SiO_4). The particle size spectrum of olivine
319 powder is shown in detail in Fig. S2. Roughly 69 % of the olivine particles, when measured by volume, fell within the

320 diameter range of 35 - 300 μm . Additionally, SEM analysis revealed high levels of Ca and O in the slag, indicative of the
 321 considerable $\text{Ca}(\text{OH})_2$ and CaO content of the powder (Table 1; please note that H cannot be measured with the applied
 322 method). The particle size measurement (Fig. S2) showed that 78 % of the ground slag particles were between 35 - 300
 323 μm .

324

325 **Table 1.** The weight percentage of elements from two minerals. Unit: wt %.

Element	O	Ca	Mn	Si	Mg	Fe	Al	Ti	Cr	Ni
Olivine	39.9	0.4		19.9	26.4	13.0	1.0			0.8
Steel slag	41.9	36.0	7.0	6.5	4.3	3.7	3.4	1.7	1.6	

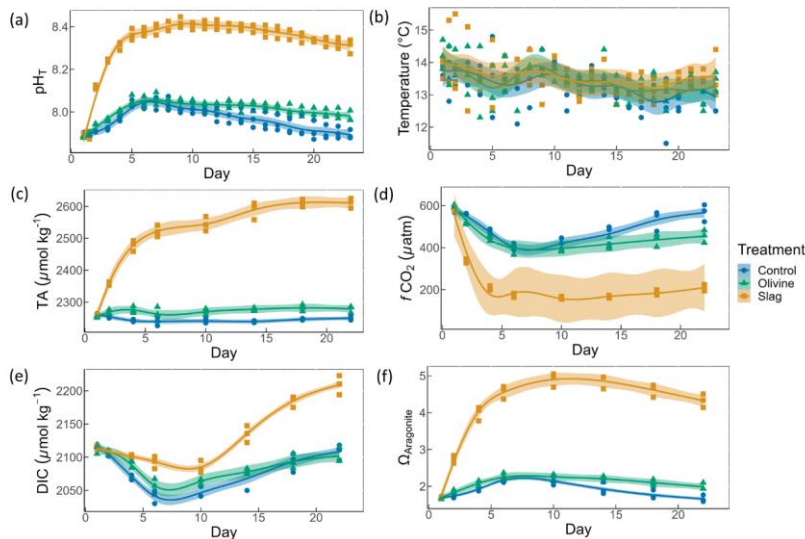
326

327

328 3.2 Physical and chemical conditions over the course of the experiment.

329 On day 2 of the experiment, when olivine particles were introduced into the microcosms, the smallest fraction of the powder
 330 remained suspended, causing the seawater to become highly turbid for several days. The resulting milky appearance of the
 331 seawater eventually faded over a period of approximately five days, and by day 5, the turbidity had visually become like
 332 the slag treatment and the control. This effect was not anticipated, and as a result, we decided to investigate its impact on
 333 light intensity. To do so, a test was conducted after the main experiment in which olivine powder was added to a microcosm
 334 identical to those used in the experiment, and light intensity was measured daily at a depth of 0.15 m. The results showed
 335 that the addition of olivine caused an initial reduction in light intensity of 18.5 % at 15 mins after addition, which declined
 336 to 7.4 %, 3.7 %, 3.7 % and 0 % after 1, 2, 3, and 4 days, respectively. These findings indicate that olivine additions can
 337 significantly affect the light environment in the microcosms, whereas no such effect was observed in the slag treatment.

338



339

340 **Fig. 2.** Carbonate chemistry conditions. The temporal development of (a) pH_T , (b) temperature, (c) total alkalinity (TA), (d) CO_2 fugacity

341 ($f\text{CO}_2$) computed at *in situ* temperature and atmospheric pressure, (e) dissolved inorganic carbon (DIC), and (f) aragonite saturation state
 342 ($\Omega_{\text{aragonite}}$). The dots represent the raw data (n=3 for each treatment per sampling time), and the fitted curve is the generalized additive
 343 model (GAM). The shading represents the 95 % confidence interval of the fitted GAM.

344

345 The pH_T of all microcosms increased from day 1 to day 5 (Fig. 2a). This was due to photosynthetic CO_2 drawdown in the
 346 control or photosynthetic CO_2 drawdown in combination with alkalinity release from minerals in the treatments. During
 347 the peak of the bloom, pH_T was 8.037 ± 0.010 in the control (average values \pm standard error), 8.054 ± 0.014 in the olivine
 348 treatment and 8.411 ± 0.015 in the slag treatment. The pH_T was significantly higher in the slag than the olivine treatment
 349 and the control throughout the experiment (control and olivine pH_T were not significantly different). The pH_T on day 23 of
 350 the control, olivine, and slag treatments were 7.893 ± 0.012 , 7.978 ± 0.015 , and 8.309 ± 0.019 , respectively. The temperature
 351 inside of the microcosms varied between replicates, which may have added noise in the biological response data. However,
 352 on average there was no statistically significant difference between control/treatments during the experiment.

353

354 In our data analysis, all the fitted GAMs from the treatments and the control exhibited significant differences in pH_T from
 355 each other, as evidenced by the p-values of both P-means and P-smooths being smaller than 0.001. For detailed results of
 356 the GAM p-values, please refer to Table S2.

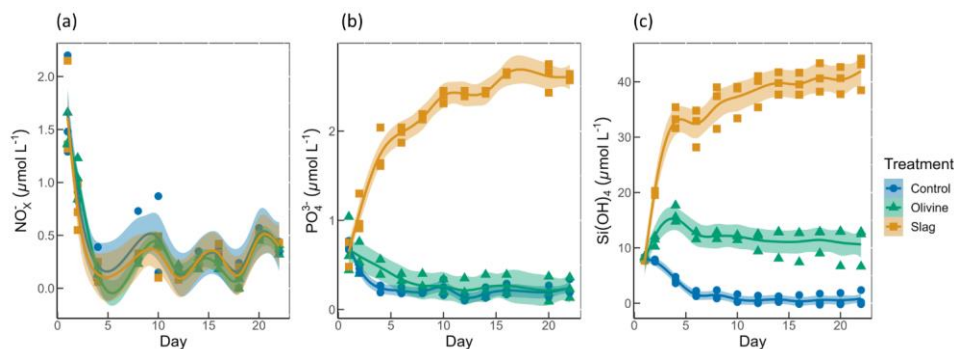
357

358 Total alkalinity increased marginally from 2255 ± 2 to $2262 \pm 13 \mu\text{mol kg}^{-1}$ within the first 6 days after olivine addition
 359 while it increased more substantially from 2259 ± 1 to $2522 \pm 11 \mu\text{mol kg}^{-1}$ in the same time span in the slag treatment (Fig.
 360 2c). The TA in the control decreased from $2261 \pm 2 \mu\text{mol kg}^{-1}$ to $2240 \pm 7 \mu\text{mol kg}^{-1}$ from day 1 to day 6 but remained
 361 stable thereafter. The TA reached $2279 \pm 6 \mu\text{mol kg}^{-1}$ in the olivine treatment and $2611 \pm 9 \mu\text{mol kg}^{-1}$ in the slag treatment
 362 on day 22. The slag treatment reached a significantly higher TA than the olivine treatment and the control (P-smooths <
 363 0.001). The mean TA from GAM in olivine treatment was higher than the control (P-means < 0.001).

364

365 The CO_2 fugacity ($f\text{CO}_2$) computed at *in situ* temperature and atmospheric pressure decreased continuously in the first 6
 366 days in all microcosms (Fig. 2d). Then it increased again in the control and olivine treatments while staying lower in the
 367 slag treatment (P-means and P-smooths ≤ 0.001 between either treatment or the control). Dissolved inorganic carbon (Fig.
 368 2e) and the aragonite saturation state ($\Omega_{\text{aragonite}}$; Fig. 2f) revealed a similar trend over the course of the experiment in the
 369 control and the olivine treatment. In contrast, the slag treatment had higher DIC and $\Omega_{\text{aragonite}}$ values throughout the
 370 experiment (P-means < 0.001).

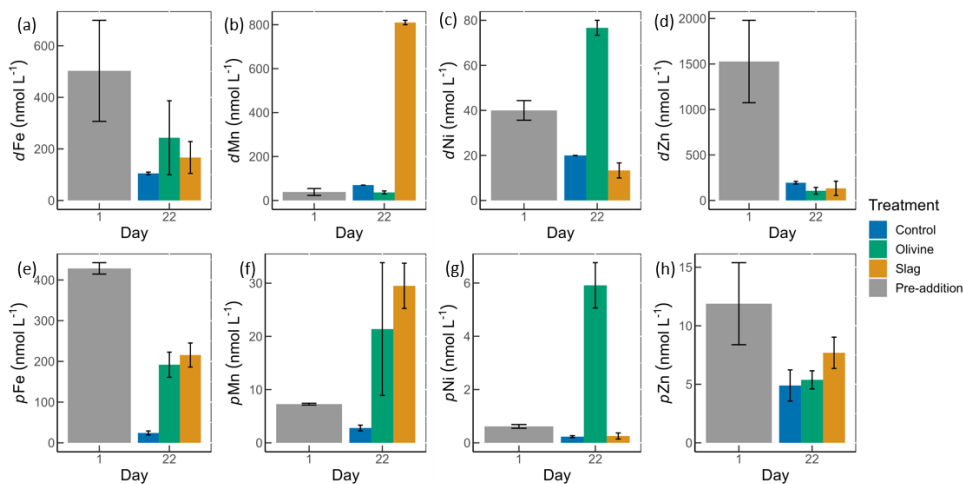
371



372 **Fig. 3.** Macronutrients concentrations over the course of the study. (a) Nitrate and nitrite concentrations. (b) Phosphate concentrations.
 373 (c) Silicic acid concentrations. The dots represent the raw data (n=3 for each treatment per collection), and the fitted curve is the
 374 generalized additive model.

375
 376 Initial nitrate and nitrite (NO_x^-), phosphate (PO_4^{3-}), and silicic acid ($\text{Si}(\text{OH})_4$) concentrations were 1.58 ± 0.12 , 0.69 ± 0.59 ,
 377 and $8.04 \pm 0.10 \mu\text{mol L}^{-1}$, respectively (Fig. 3). NO_x^- declined rapidly in all microcosms once the experiment had
 378 commenced to values below $0.5 \mu\text{mol L}^{-1}$ and no significant difference was detected between treatments and control (P-
 379 smooths >0.05 ; Fig. 3a). In both the olivine treatment and the control, the PO_4^{3-} concentration decreased in the first six
 380 days (Fig. 3b). In the slag treatment, PO_4^{3-} increased to a maximum of $2.65 \pm 0.01 \mu\text{mol L}^{-1}$, which was significantly higher
 381 than in the olivine treatment and the control (P-means <0.001). The $\text{Si}(\text{OH})_4$ concentration increased to a maximum of
 382 $15.99 \pm 0.87 \mu\text{mol L}^{-1}$ in the olivine treatment, increased to a maximum of $41.92 \pm 1.75 \mu\text{mol L}^{-1}$ in the slag treatment, but
 383 decreased below the detection limit in the control (Fig. 3c). Significant differences were observed in the development of
 384 $\text{Si}(\text{OH})_4$ between all treatments and the control (Table S2).

385



386
 387
 388 **Fig. 4.** Dissolved and particulate trace metal concentrations in microcosm seawater. (a)-(d) are dissolved trace metal concentrations, and
 389 (e)-(h) are total particulate trace metal concentrations. The error bars represent the standard error from measured samples. The pre-
 390 addition data shown in (a)-(d) represent the average of 7 microcosms before addition of slag or olivine. The data for the control on day
 391 22 in (a)-(d) and for the pre-addition on day 1 in (e)-(h) were based on two of three microcosm replicates. The remaining data were based
 392 on all three microcosm replicates.

393

394 The dissolved trace metal concentrations measured from microcosms are presented in Fig. S3. While the mass of olivine
 395 added to the microcosms was 50-fold greater than in steel slag (100 g vs 2 g), it's noteworthy that the variation in dissolved
 396 trace metal concentrations between the two treatments were much smaller than 50 folds. After 21 days of experiment, the
 397 treatments showed an increase in dissolved Al concentrations from 920 ± 286 to $970 \pm 228 \text{ nmol L}^{-1}$ in olivine treatment,
 398 and from 920 ± 286 to $1093 \pm 77 \text{ nmol L}^{-1}$ in slag treatment, while in the control dissolved Al decreased to $230 \pm 10 \text{ nmol}$

399 L⁻¹ (Fig. S3). The fitted GLMs were compared, and the p-value revealed how much influence a treatment had on the
400 dissolved metal concentrations (Table S3). The results indicate that the slag and olivine additions led to significantly higher
401 Al concentrations than in the control (p-values < 0.05), but no significant difference was found between the two treatments
402 (p-value = 0.189). The Cu concentration in the olivine on day 22 was significantly higher than the slag treatment and the
403 control (p-value < 0.05) (Fig. S3). The addition of olivine and slag released some dissolved Fe, but overall, the concentration
404 of Fe did not differ significantly between treatments (Fig. 4a, Table S3). The slag released a substantial amount of dissolved
405 Mn (maximum 810 ± 10 nmol L⁻¹ on day 22) (Fig. 4b), leading to significantly higher concentrations than in the olivine
406 treatment and the control (p-values < 0.001). A significant amount of dissolved Ni (maximum 77 ± 3 nmol L⁻¹ on day 22)
407 was released from the olivine powder (p-values < 0.001) (Fig. 4c). The initial concentration of dissolved Zn in seawater
408 was much higher than on day 22 in all microcosms, and no significant difference in Zn concentrations was found between
409 the treatments and the control.

410

411 Particulate concentrations of some trace metals also differed between treatments. The total particulate Fe decreased in all
412 microcosms on day 22 comparing with the pre-addition level, but both mineral addition treatments had higher particulate
413 Fe concentrations than the control (Fig. 4e). The addition of slag elevated particulate Mn concentrations to a level higher
414 than the pre-addition and the control on day 22 (Fig. 4f), while the addition of olivine increased the particulate Ni
415 concentrations to a level higher than the slag, the control, and the pre-addition (Fig. 4g). The particulate Zn concentrations
416 in general decreased by the end of the experiment (Fig. 4h), and no significant differences were found between the
417 treatments and the control.

418

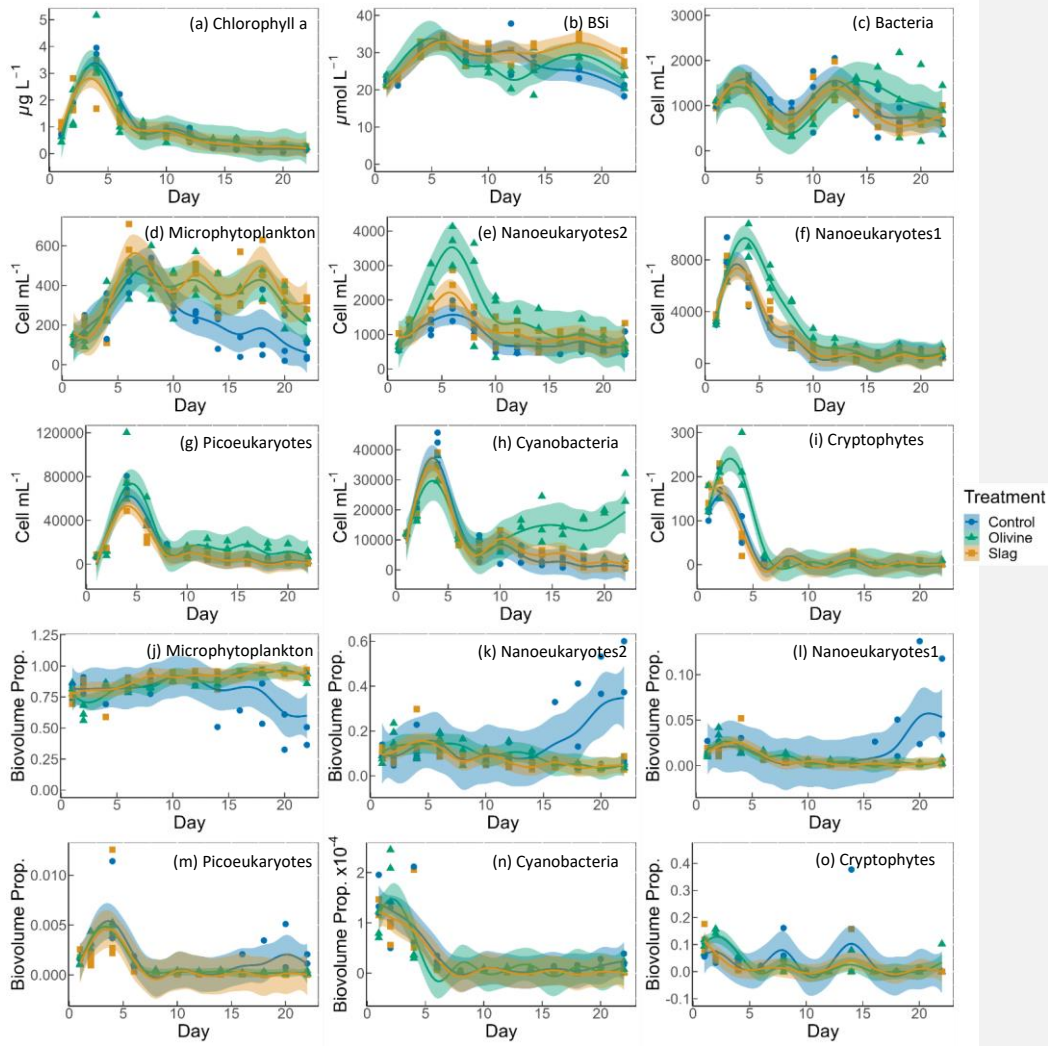
419 The POC on day 1 and day 22 from all microcosms were very similar, 10.99 ± 0.58 and 11.03 ± 0.41 μmol L⁻¹ respectively
420 (Fig. S4) so the metal:POC results were consistent with the particulate trace metal results (Fig. 4 e-h). In general, the non-
421 surface metal:POC are positively correlated with the total metal:POC ratios (Fig. S5). The ratio of non-surface to total
422 particulate trace metal concentrations is summarized in Table S5. Both non-surface and total Fe concentrations decreased
423 in microcosms on day 22 compared with the pre-addition level. Iron:POC ratios were significantly higher in the treatments
424 than in the control on day 22 (p-values < 0.05, Table S3), and there was no significant difference between mineral addition
425 treatments. The non-surface to total Fe:POC ratios were > 0.94 in all microcosms on both day 1 and day 22. The total and
426 non-surface Mn:POC ratio was the highest in the slag treatment. These ratios were higher than the pre-addition level and
427 the control at the end of the experiment. The total particulate Ni concentrations in the olivine treatment were significantly
428 higher than before olivine addition. The olivine treatment led to a >22-fold higher Ni:POC ratio compared to the other two
429 treatments (p-value < 0.001).

430

431

432

433 3.3 Development and physiology of the plankton community



434
 435 **Fig. 5.** Temporal development of chlorophyll a concentration (chl-a), BSi, and different eukaryotic and bacterial plankton groups as
 436 determined with flow cytometry. (a) chlorophyll a; (b) BSi; cell concentrations of (c) heterotrophic bacteria, (d) microphytoplankton, (e)
 437 nanoeukaryotes2, (f) nanoeukaryotes1 (g) picoeukaryotes, (h) cyanobacteria, and (i) cryptophytes; biovolume proportion of (j)
 438 microphytoplankton, (k) nanoeukaryotes2, (l) nanoeukaryotes1 (m) picoeukaryotes, (n) cyanobacteria, and (o) cryptophytes. The figure
 439 data points represent the raw data, and the fitted curve is the generalized additive model. The shaded area represents the 95 % confidence
 440 interval.
 441

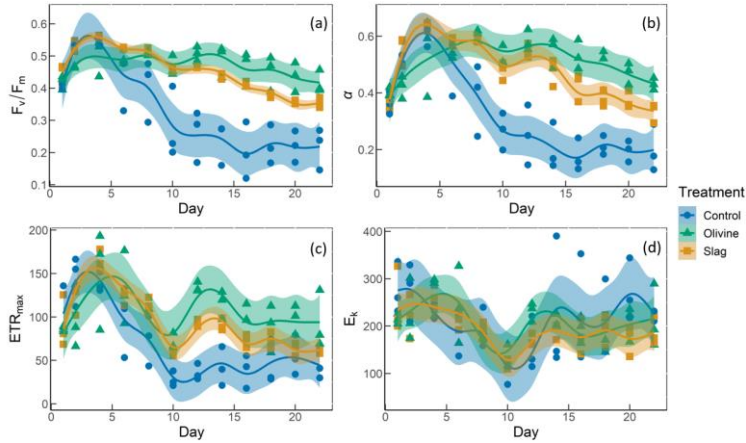
442 The chl-a concentration in all microcosms increased from day 1 to day 4 from $1 \mu\text{g L}^{-1}$ to $3\text{-}4 \mu\text{g L}^{-1}$ (Fig. 5a). The chl-a
443 concentration then decreased rapidly from day 4 to day 8, then continued to decrease, though more slowly, to $<0.3 \mu\text{g L}^{-1}$
444 until the end of the experiment. The GAMs of chl-a did not show any difference between treatments and the control (both
445 P-means and P-smooths >0.05 , see Table S2).

446
447 The BSi concentration increased from day 1 to day 6 in all microcosms (Fig. 5b). In the olivine treatments, BSi
448 concentrations decreased slightly after the peak until day 12 but then increased again. In the slag treatment, BSi
449 concentrations remained relatively stable after the initial phytoplankton bloom. In contrast, BSi concentration decreased
450 continuously in the control after the initial peak. Olivine particles suspended in seawater after the mineral addition (see
451 section 3.2) partially ended up on BSi filters during filtration. This led to extremely high BSi measurements on days 2 and
452 4 that were removed from Fig. 5b. Without these outliers, the mean of fitted BSi GAM in the olivine treatment was lower
453 than the control and the slag treatment (Table S2), and the slag treatment had the highest average BSi over the course of
454 the experiment. Overall, the BSi trends in the two treatments were similar (P-smooths = 0.269), and both were significantly
455 different from the control (P-smooths <0.05).

456
457 The development of the phytoplankton community composition showed significant differences between the treatments and
458 the control. In general, most phytoplankton groups exhibited similar patterns to chl-a, with peak cell numbers occurring on
459 day 4 (Fig. 5f-i) apart from microphytoplankton and nanoeukaryotes2 which had the peak delayed for 1-2 days (Fig. 5d-
460 e). Please be aware that flow cytometers may not capture some large and chain-forming phytoplankton. After reaching
461 peak values during the bloom, phytoplankton abundance generally decreased steadily. Microphytoplankton displayed
462 similar trends to the results for BSi. Before day 10, all microcosms had similar microphytoplankton abundances (Fig. 5d).
463 However, in the control, microphytoplankton abundance declined continuously and at a faster rate compared to the two
464 treatments (P-smooths values <0.03). From day 2 to day 6, the abundance of nanoeukaryotes1, nanoeukaryotes2,
465 picoeukaryotes, and cryptophytes was higher in the olivine treatment compared to the slag treatment and the control. After
466 day 8, their abundance in the olivine treatment decreased to a similar level as the slag treatment and the control. Notably,
467 there were few significant differences observed between the slag treatment and the control in terms of the abundances of
468 nanoeukaryotes1, nanoeukaryotes2, picoeukaryotes, cyanobacteria, and cryptophytes throughout the experiment. In the
469 olivine treatment, cyanobacteria experienced a second bloom after day 10, which was significantly different from the other
470 two groups (P-smooths <0.01). Heterotrophic bacteria exhibited an increase and decline pattern following the
471 phytoplankton bloom until day 8 (Fig. 5c). Subsequently, bacteria abundance increased again, reaching a second peak
472 during days 12-14, followed by a decline until the end of the experiment. The decline in bacteria abundance was slower in
473 the olivine treatment, although no significant differences were detected between treatments (Table S2).

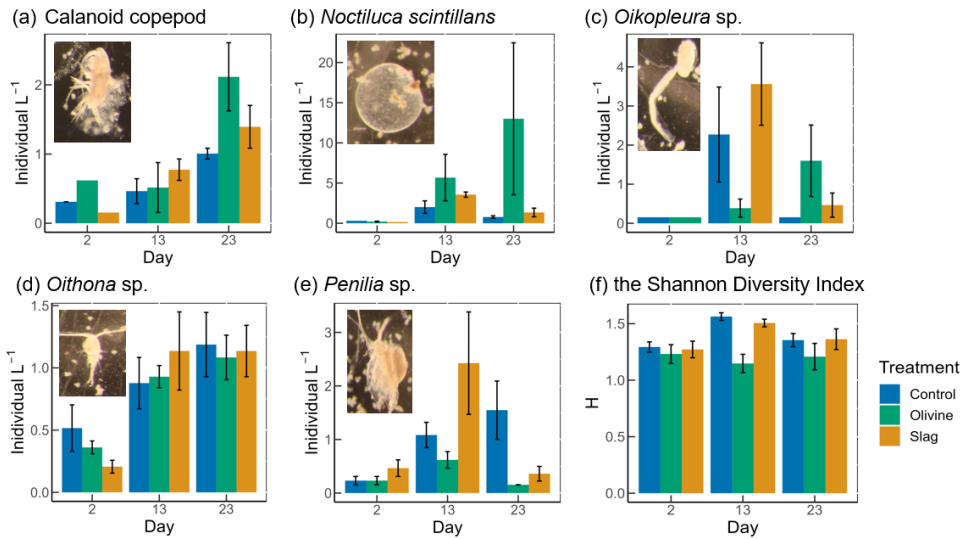
474
475 Among all the microcosms, microphytoplankton consistently accounted for the largest proportion of biovolume. From the
476 perspective of biovolume proportion, the mineral addition mainly influenced the microphytoplankton and nanoeukaryotes.
477 The control had similar phytoplankton biovolume distribution as the treatments from day 1 to day 15, but after that the
478 proportion of microphytoplankton biovolume decreased to a level significantly lower than the treatments. In the control
479 treatment, the proportion of nanoeukaryotes' biovolume increased as the proportion of microphytoplankton decreased. The
480 biovolume of picoeukaryotes, cyanobacteria and cryptophytes increased during the phytoplankton bloom and then
481 decreased drastically after the bloom. There were no significant differences in biovolume proportion observed for

482 picoeukaryotes, cyanobacteria and cryptophytes between the treatments and the control.
 483



484
 485 **Fig. 6.** The photosynthetic performance of the phytoplankton community. (a) F_v/F_m , the maximum quantum yield of photosynthesis II.
 486 (b) α , the initial slope of the rapid light curves. (c) ETR_{max} is the maximum electron transport rate, the maximum potential photosynthetic
 487 rate. (d) E_k is light-saturation parameter, Unit: $\mu\text{mol photons m}^{-2} \text{s}^{-1}$.
 488

489 The temporal development of F_v/F_m , α , ETR_{max} , and E_k is illustrated in Fig. 6. The F_v/F_m values of the phytoplankton
 490 community were approximately 0.42 ± 0.01 and increased to levels > 0.5 during the peak of the phytoplankton bloom on
 491 day 4 (Fig. 6a). Following the bloom, F_v/F_m values dropped below 0.3 in the control. However, the decline in F_v/F_m after
 492 the bloom was less pronounced in the two mineral addition treatments with the olivine treatment maintaining higher F_v/F_m
 493 values than the slag treatment (P-smooths < 0.05). At the end of the experiment, F_v/F_m was 0.22 ± 0.04 in the control, 0.35
 494 ± 0.01 in the slag treatment, and 0.42 ± 0.02 in the olivine treatment. The temporal development of α aligned with the
 495 patterns observed for F_v/F_m (compare Fig. 6a and 6b). The maximum values of ETR_{max} were observed on day 4 in the
 496 control and the slag treatment, while in the olivine treatment, it occurred on day 5 (Fig. 6c). Subsequently, ETR_{max}
 497 continuously decreased until day 10 and then stabilized until the end of the experiment. However, ETR_{max} exhibited a
 498 subsequent increase in the mineral treatments around day 12. The ETR_{max} values were higher in the mineral treatments
 499 compared to the control group (P-means < 0.001 , Table S2). The parameter E_k decreased from $246 \pm 17 \mu\text{mol photons m}^{-2}$
 500 s^{-1} on day 1 to $121 \pm 7 \mu\text{mol photons m}^{-2} \text{s}^{-1}$ on day 10, and then it increased again to approximately $200 \mu\text{mol photons m}^{-2}$
 501 s^{-1} by the end of the experiment (Fig. 6d). The change in E_k did not exhibit significant differences between the treatments
 502 and the control (both P-means and P-smooths > 0.05).
 503
 504



505 **Fig. 7.** The dominant zooplankton abundance and community diversity from different treatments. Abundance of dominant zooplankton
 506 in microcosms: (a) calanoid copepod; (b) *Noctiluca scintillans*; (c) *Oikopleura* sp.; (d) *Oithona* sp.; (e) *Penilia* sp.; and (f) the Shannon
 507 diversity index (H) of different treatments and the control. Error bars represent the standard error calculated from three microcosm
 508 replicates. Photographs of each zooplankton group are shown on the corresponding graphs.
 509

510
 511 Thirteen zooplankton taxonomic groups were identified in the microcosms. The dominant taxa were the appendicularian
 512 *Oikopleura* sp., the cyclopoid copepod *Oithona* sp., the cladoceran *Penilia* sp., the heterotrophic dinoflagellate *Noctiluca*
 513 *scintillans* and several calanoid copepods including *Acartia* sp., *Paracalanus* sp. and *Gladioferens* sp. The larvae and eggs
 514 of *Oikopleura*, *Penilia* and copepod were also observed under the microscope. In general, higher zooplankton numbers
 515 were observed after the bloom on day 13 (Fig. 7). The abundance of calanoid copepods and *Oithona* sp. increased after
 516 day 2 (Fig. 7a, d), and there was no significant difference between treatments and the control (p-values >0.05, Table S4).
 517 The abundance of *N. scintillans* increased significantly more in the olivine treatment than in the control and the slag
 518 treatment, with highest abundance of 13 ± 9 individual L^{-1} observed in the olivine treatment on the last day (Fig. 7b). The
 519 abundance of *Oikopleura* in the control and the slag treatment was higher than the olivine treatment on day 13 but was
 520 higher in the olivine treatment on day 22 (Fig. 7c). A higher abundance of *Penilia* sp. was found in the slag treatment on
 521 day 13 and in the control on day 23 (Fig. 7e). Due to the patchy distribution of zooplankton, these data have large standard
 522 errors and only the differences in the numbers of *N. scintillans* in the olivine treatment were statistically significantly
 523 different from the slag treatment and the control (p-value <0.05, Table S4).
 524

525 Considering the control and slag treatment, the Shannon Diversity Index (H) increased from day 2 to day 13 and declined
 526 on day 23, while in the olivine treatment, H was lower on day 13 than on day 2 and day 23 (Fig. 7f). The GLMs revealed
 527 that the olivine treatment had significantly lower H on day 13 than the control and the slag treatment (p-values <0.001).
 528 There were no significant differences in H between the control and the slag treatment (Table S4). The addition of olivine
 529 decreased the zooplankton community's diversity. This is mainly driven by distinct trends observed in the abundance of
 530 *Oikopleura* sp., *Penilia* sp., and *N. scintillans* (Fig. 7).

531

532 4. Discussion

533 4.1 CO₂ removal potential of slag and olivine

534 The slag powder created significantly higher CO₂ removal potential than the olivine powder over the course of the study.
535 Ca(OH)₂ and CaO in slag and Mg₂SiO₄ in olivine are likely to be the main functional minerals driving the measured
536 alkalinity enhancement. Total alkalinity increased by 361 μmol kg⁻¹ in the slag treatment while it increased by only 29
537 μmol kg⁻¹ in the olivine treatment, equivalent to a potential increase in marine inorganic carbon by 14.7 and 0.9% within
538 3 weeks of their application. When normalizing these alkalinity increases to the same material weight, 1 g of slag would
539 release 9626 μmol TA while 1 g of olivine would release 16 μmol TA. Thus, over 3 weeks of experimental incubation, slag
540 is ~600-fold more efficient in releasing alkalinity for particles of this size class (please note that particle size spectra of
541 olivine and slag were similar but not identical; Fig. S1). We can also use these values to make a rough estimate of how
542 much CO₂ these two minerals could potentially sequester. One mole of alkalinity from olivine and slag can sequester
543 approximately 0.85 mole of CO₂. Thus, one tonne of slag and olivine powder as used here could sequester 360 and 0.6 kg
544 CO₂, respectively, within 3 weeks. Please note, however, that the amount of olivine added to the experiments (1.9 g L⁻¹)
545 contains substantially more alkalinity in solid phase than the slag and that this alkalinity could be released over longer
546 timescales so that the CDR efficiency of olivine could increase more substantially than slag over time. Furthermore, it is
547 likely that optimization of particle size and application method may lead to higher efficiencies of the slag but especially of
548 the olivine with its inherently slower dissolution rate. Nevertheless, the slag showed potential as an OAE source mineral,
549 even when applied as relatively coarse powder in this experiment.

550

551 4.2 Environmental implications of slag and olivine additions

552 The amount of olivine and slag powder added to the treatments differed significantly (100 g of olivine powder were added
553 while only 2 g of slag powder were added to the 53 L microcosms). Our rationale for these different mass additions was to
554 yield somewhat similar amounts of detectable alkalinity enhancement in the dissolved phase, since we already knew from
555 tests before the experiment that slag elevates alkalinity faster than olivine. However, olivine was less efficient in releasing
556 alkalinity than we had anticipated so that even a 50-fold higher addition of olivine (in mass) did not compensate for this
557 difference. As such, our experiments are associated with an “apples and oranges issue” in that our perturbation with
558 minerals and associated OAE differs. To account for this, the following discussion mainly relates the observed
559 environmental effects with the alkalinity enhancement achieved over the course of the study.

560 4.2.1. OAE effects on phytoplankton physiology and community

561 Previous research has hypothesised that OAE-induced changes in seawater carbonate chemistry could delay phytoplankton
562 bloom formation due to reductions in seawater pCO₂ in the aftermath of an OAE deployment (Bach et al., 2019). The build-
563 up of chlorophyll *a* concentration as observed here was indistinguishable between treatments and the control, suggesting
564 no effect of slag- or olivine-based OAE on phytoplankton bloom dynamics under these experimental settings. A lack of
565 bloom delay due to carbonate chemistry is unsurprising for the olivine treatment where the release of alkalinity was small

Formatted: Subscript

Formatted: Superscript

566 (29 $\mu\text{mol kg}^{-1}$ alkalinity release), but somewhat more surprising in the slag treatment where alkalinity was quite rapidly
567 increased by 361 $\mu\text{mol kg}^{-1}$. However, the release was still lower than in a very similar study by Ferderer et al., (2022)
568 where alkalinity was increased by 500 $\mu\text{mol kg}^{-1}$ using sodium hydroxide and even there they did not observe a bloom
569 delay. Based on this very limited evidence, it seems that bloom delays do not occur consistently under OAE within the
570 alkalinity ranges tested in this study.

571

572 The nutrient data show that the phytoplankton community was most likely N-limited after day 4 so that the release of
573 Si(OH)_4 from olivine and Si(OH)_4 and PO_4^{3-} from slag did not stimulate a further increase in chlorophyll-*a* concentration
574 in the treatments. The development of BSi concentrations is indicative of the prevalence of diatoms in the microcosms but
575 differences between treatments and the control were small. The release of Si(OH)_4 through olivine and slag will most likely
576 benefit diatoms but this fertilization effect did not manifest in this specific experiment because N was limiting diatom
577 growth. However, when new N is supplied then diatoms will likely take a bigger share of the limiting N pool when olivine
578 or slag are used for OAE, as has been shown in Si(OH)_4 manipulation experiments in and outside the context of OAE
579 research (Egge and Jacobsen, 1997; Ferderer et al., 2023). In the case of slag, the release of PO_4^{3-} will likely be another
580 driver that affects plankton productivity and community composition. As for Si(OH)_4 , however, the effect of additional
581 PO_4^{3-} did likely not materialise in this experiment because PO_4^{3-} was not limiting over the course of the study. However, in
582 ecosystems where PO_4^{3-} is a limiting resource, the application of slag could enhance productivity with associated benefits
583 for higher trophic levels. In contrast, excessive applications of slag and concomitant PO_4^{3-} release could also pose a risk of
584 eutrophication. Future studies may need to investigate what the most sustainable dose of OAE via olivine and/or slag
585 applications could be and the suitable regions for application.

586

587 The flow cytometry results further revealed the change in phytoplankton community composition. Both the olivine and
588 slag treatments sustained higher microphytoplankton abundances after the peak of the phytoplankton bloom. This trend is
589 consistent with higher F_v/F_m values in the treatments than in the control so that it is tempting to assume that
590 photophysiological fitness gain measured with the FRRf led to higher competitiveness of microphytoplankton in the
591 community. Indeed, calculations of the contribution of different phytoplankton groups to total biovolume based on flow
592 cytometry indicate that microphytoplankton were predominantly contributing to the phytoplankton community biovolume
593 so that the responses measured by the FRRf were probably to a large extent driven by this group.

594

595 Apart from the increased microphytoplankton abundance, for the slag treatment, other phytoplankton groups distinguished
596 with flow cytometry did not deviate considerably from the control. The olivine addition, however, triggered more
597 pronounced shifts in the phytoplankton community. In particular, the nanoeukaryotes (roughly between 2-20 μm),
598 picoeukaryotes and the cryptophytes showed relatively higher abundance during the peak of the phytoplankton bloom, and
599 the abundance of cyanobacteria was higher after the bloom. We speculate that this shift following olivine treatment may
600 be attributable to a top-down effect from the decrease in zooplankton grazing effects in microcosms, which will be
601 discussed in section 4.2.2.

602

603 The measurement of photophysiological parameters revealed that the phytoplankton had generally better photosynthetic
604 performance in the slag and olivine treatments than in the control, especially after the phytoplankton bloom. During the
605 first 5 days, the changes in phytoplankton photosynthetic performance were indistinguishable between the control and the

606 slag treatment, while the values of α , ETR_{max} and F_v/F_m were lower in olivine treatment. At this time all microcosms had
607 similar health because of the relatively high NO_x^- concentrations and Fe supply (around 500 nmol L^{-1}), but the suspended
608 particles in the olivine treatment may have led to artifacts in the measuring of photophysiology by FRRf. Scattering and/or
609 absorption of light by suspended olivine particles is the most parsimonious explanation for the simultaneous depression in
610 α , ETR_{max} and F_v/F_m . After day 5, the F_v/F_m , α and ETR_{max} values decreased significantly faster in the control than in the
611 treatments, and to values lower than the initial condition. A decrease of F_v/F_m is commonly associated with physiological
612 stress, such as nutrient limitation, and high light stress (Bhagooli, et al., 2021), with Fe limitation causing a more
613 pronounced decline in F_v/F_m than nitrogen limitation (Gorbunov, et al., 2021). The ETR_{max} , which represents the maximum
614 electron transport rate, has also been shown to be negatively affected when phytoplankton experience nitrogen or Fe
615 limitation (Kolber et al., 1994; Gorbunov & Falkowski 2021). Furthermore, the change in photosynthesis performance
616 after day 10 was suspected to be driven by the microphytoplankton because the decrease of F_v/F_m , α , and ETR_{max} in the
617 control was coupled with the decrease in microphytoplankton abundance while the other phytoplankton groups were in
618 low abundance as in the mineral addition treatments, and the microphytoplankton contributed significantly (75 %) to
619 community biovolume. All microcosms were similarly NO_x^- limited from day 5 onward (Fig. 3) so that N-limitation is
620 unlikely to explain different trends in photophysiological parameters between the control and OAE treatments. Trace metals,
621 especially Fe, released through slag and olivine additions could potentially explain these differences.

622
623 Several of the trace metals released from slag and olivine are required for photosynthesis. For example, Fe is required for
624 many proteins functioning in photosynthesis, such as cytochromes, ferredoxin, and superoxide dismutase (SOD) (Twining
625 and Baines, 2013), and the addition of Fe can stimulate the growth of phytoplankton (Sunda and Huntsman, 1997) and
626 increase F_v/F_m (Behrenfeld et al., 2006). The dissolved and particulate Fe concentrations were higher in mineral addition
627 treatments than in the control indicating potentially more Fe available to sustain phytoplankton photosynthesis. While this
628 explanation is intriguing for the observed trends in photophysiology, it remains unclear why such strong differences
629 occurred between mineral addition and control treatments despite dissolved Fe concentrations of $\sim 500 \text{ nmol L}^{-1}$ at the end
630 of the experiment in the control. In Fe-limited ocean regions, dissolved Fe is at least two orders of magnitude lower, and
631 the enhancement of Fe to $\sim 1.5 \text{ nmol L}^{-1}$ can induce major phytoplankton blooms and relieve photophysiological stress (De
632 Baar et al., 2005). It is possible that these coastal phytoplankton species have higher Fe requirements than those from the
633 open ocean where Fe is limiting (Strzepek and Harrison, 2004). Our findings suggest that Fe perturbations may not only
634 be relevant for low Fe open ocean regions but could also be relevant for coastal ocean locations.

635
636 Alternatively, the addition of Mn, Ni and other trace metals from mineral addition may have benefited photosynthesis.
637 Manganese is required for the water-splitting reaction of photosystem II (Armstrong, 2008), and both Mn and Ni are
638 common bioactive trace metals for SODs in marine phytoplankton. The noxious superoxide anion radical (O_2^-) generated
639 from aerobic respiration and oxygenic photosynthesis could be harmful to phytoplankton physiology, and SOD removes
640 O_2^- , thus improving photosynthesis (Wafar et al., 1995; Wolfe-Simon et al., 2005). This is consistent with our
641 photosynthetic measurements. Interestingly, although the amounts and types of trace metals released from the slag and
642 olivine powders were different, they led to relatively similar F_v/F_m values with only slightly higher F_v/F_m in the olivine
643 than the slag treatment from days 10-21. Over this time, these trace metal additions could have fertilized different
644 phytoplankton species (Pausch et al., 2019; Balaguer et al., 2022; Guo et al., 2022) possibly because different
645 phytoplankton could have different trace metal requirements, such as for SOD. For example, cyanobacteria have NiSOD,

646 diatoms have MnSOD, dinoflagellates have both FeSOD and MnSOD (Wolfe-Simon et al., 2005). Another explanation is
647 that phytoplankton in the control were limited by bicarbonate while the treatments had sufficient bicarbonate from added
648 minerals. However, we were unable to determine the species-level changes in the phytoplankton community, and hence
649 whether these trace metals, individually or combined, could account for the observed phytoplankton community
650 photosynthetic performance.

651

652 **4.2.2. OAE impacts on the zooplankton community**

653 Slag-based OAE did not significantly influence the zooplankton community composition while olivine-based OAE induced
654 some statistically significant effects, including a lower Shannon diversity. The increase in *N. scintillans* abundance and the
655 decrease in *Penilia* sp. and *Oikopleura* sp. in the olivine treatment indicate that the zooplankton response to OAE can vary
656 among different zooplankton types.

657

658 The observed lower abundance of *Oikopleura* sp. on day 13 in the olivine treatment may indicate a temporary suppression
659 or a slower growth rate of this zooplankton species in response to the olivine addition. This could be attributed to the
660 potential effects of olivine on the availability of essential nutrients or changes in the physicochemical environment of the
661 water. However, the subsequent increase in *Oikopleura* sp. abundance by day 22 suggests that the growth of this species
662 may have recovered or accelerated in the olivine treatment, leading to a higher abundance compared to the slag treatment
663 and the control on day 22. As discussed in section 4.2.1, reduced *Oikopleura* sp. abundance was unlikely due to reduced
664 food availability since phytoplankton within the preferred edible size spectrum, such as cyanobacteria and nanoeukaryotes,
665 were even more abundant in the olivine treatment. Instead, we hypothesize it to be an effect of the suspended olivine
666 particles that occurred for approximately the first 5 days of the study that were so plentiful that they turned the enclosed
667 seawater milky and may have clogged the mucous feeding mesh of *Oikopleura* sp. (Lombard et al., 2011).

668

669 The abundance of *Penilia* sp. and *Oikopleura* sp. was lower in the olivine treatment than the other two groups throughout
670 the experiment while the abundance of *N. scintillans* was consistently higher. The second bloom of cyanobacteria in olivine
671 is potentially the results of decreased predators, like *Penilia* sp. and *Oikopleura* sp.. We cannot provide a particularly
672 convincing hypothesis about what specifically drove these in these zooplankton species, although it is tempting to speculate
673 that suspended particles present in the olivine treatment at the beginning may have played a role also for those organisms
674 since this was the only apparent systematic difference to the control and slag treatment. The proliferation of *N. scintillans*
675 can be problematic since heterotrophic dinoflagellate blooms can regulate phytoplankton communities, cause toxicity to
676 aquatic fish, and create a hypoxic sub-surface zone (Baliarsingh et al., 2016; Zhang et al., 2020; Al-Azri et al., 2007),
677 although a bloom of *N. scintillans* in southeast Australia only induced ichthyotoxicity when the cell concentration reached
678 2,000,000 cells L⁻¹ (Hallegraeff et al., 2019). For comparison, we observed a maximum of 32 cells L⁻¹ in one microcosm
679 replicate of the olivine treatment.

680

681 In comparison to olivine, steel slag seemed to have less potential to affect zooplankton community composition. The
682 abundance of all groups of phytoplankton, apart from microphytoplankton after day 10, was similar in the slag treatment
683 and the control through the experiment. This is probably because the amount of slag powder added in the treatment was
684 much less than the olivine powder resulting in fewer physical particle perturbations to zooplankton. In addition, the

685 chemistry perturbations such as enhanced alkalinity concentration and various dissolved trace metals, especially Mn, from
686 the slag powder did not seem to have a notable direct influence on zooplankton abundance over the three-week period.
687 Even though we did not observe drastic changes in zooplankton abundance during the experiment, considering there was
688 higher microphytoplankton abundance in the slag treatment after day 10, slag powder may benefit some zooplankton
689 especially those who feed on large phytoplankton on a longer time scale.
690

691 **4.2.3. Dissolved trace metal accumulation in seawater and its environmental implications**

692 The addition of olivine and slag as OAE source minerals released trace metals into the seawater, predominantly Al, Fe, Ni,
693 and Cu (olivine) as well as Al, Fe, and Mn (slag). The maximum measured concentrations for dissolved Al, Fe, Ni, Cu, and
694 Mn were 1093, 253, 77, 27, and 810 nmol L⁻¹, respectively. The threshold values for drinking water with health or aesthetic
695 considerations by the Australian Drinking Water Guidelines for Al, Fe, Ni, Cu, and Mn are 7400, 5360, 340, 15600, and
696 1800 nmol L⁻¹, respectively (NRMCC, 2022). All dissolved trace metal concentrations measured herein are well below
697 these health and aesthetic threshold values. In natural freshwater sources, the concentrations of Al, Fe, Ni, Cu and Mn are
698 generally less than 44000, 71400, 510, 156, and 25400 nmol L⁻¹ (NRMCC, 2022). Although these natural water data were
699 primarily derived from rivers and streams, they serve as valuable references for evaluating trace metal release in our
700 experiment. Thus, mineral additions to the microcosms as simulated here did not increase thresholds for any of the
701 measured trace metals beyond those that are considered safe for drinking water quality, and they were within the trace
702 metal concentration range in natural water. However, while these guidelines on drinking water provide a good starting point
703 on how to quantify what OAE perturbation could be considered “safe” and “unsafe” with regards to trace metals, it must
704 be recognized that seawater is not drinking water and that critical thresholds may be different in the latter.
705

706 The release of trace metals from OAE materials is considered to have relatively strong effects on biology, particularly in
707 the open ocean where trace metals usually occur in lower concentrations. For example, oceanic Al, Fe, Ni, and Mn
708 concentrations are about 2, 0.5, 8, and 0.3 nmol L⁻¹ (Bruland and Lohan, 2003; Sohrin and Bruland, 2011). Previous
709 research on OAE-associated trace metal impacts on individual phytoplankton species grown in laboratory environments
710 has shown that concentration thresholds beyond which trace metal induces negative effects on fitness likely differ between
711 species (Guo et al., 2022; Hutchins et al., 2023; Xin et al., 2023). Indeed, our experiment with plankton communities
712 provides further support that several components of the planktonic food web are affected by OAE. However, our experiment
713 does not allow determining whether observed effects were primarily invoked by carbonate chemistry, macronutrient (P and
714 Si), or trace metal perturbations. Thus, dedicated experiments isolating the impact of these factors on plankton will be
715 required in the future.

716 **4.2.4. Particulate trace metal accumulation in seawater and its environmental implications**

717 The Derwent Estuary (where we collected our plankton communities) was highly metal polluted due to industrial practice
718 (Macleod and Coughanowr, 2019). Both our dissolved and particulate trace metal data indicated high background metal
719 concentrations, especially for Fe and Zn. Furthermore, the metal:POC ratios found here are higher than reported for open
720 ocean studies or lab cultures. For example, the Fe:POC can vary from 2-136 $\mu\text{mol mol}^{-1}$ depending on the cultured
721 phytoplankton species and the environmental dissolved Fe concentration (Kulkarni et al., 2006; Sunda and Huntsman,
722 1995; King et al., 2012; Boyd et al., 2015). In our results the Fe:POC values ranged from 1200 to 39 000 $\mu\text{mol mol}^{-1}$, which

723 may be due to the particulate trace metal richness of the Derwent Estuary (control) and/or the addition of lithogenic particles
724 (slag and olivine treatment). The presence of abiotic particulate metal sources creates challenges to quantify metal quotas
725 and then to evaluate metal accumulation effects on biological organisms.

726
727 Our study reveals that the added minerals enriched the particulate trace metal pools to various degrees. Consistent with the
728 dissolved trace metal data, the slag treatment was enriched with particulate Fe and Mn while the olivine treatment was
729 enriched with particulate Fe and Ni. The enhanced particulate Ni and Mn concentrations were higher than before mineral
730 additions and the control levels. This is in line with previous research which indicates a positive correlation between
731 particulate and dissolved trace metal concentrations (Gaulier et al., 2019).

732
733 Based on the amounts released through OAE as simulated herein, it appears that Ni and Mn have the highest potential to
734 cause toxicity in certain marine organisms (Jakimska et al., 2011). These trace metals have the potential to accumulate in
735 marine organisms over time (bioaccumulation effects), and their increased concentrations in the food chain can lead to
736 adverse effects on the health and well-being of organisms at higher trophic levels (biomagnification effects). One crucial
737 next step will be to investigate whether the enhanced dissolved/particulate trace metal will affect higher trophic levels to
738 estimate the environmental risks of OAE on other marine organisms.

739

740 **5 Conclusions**

741 Our study aimed to assess the environmental impacts of two ground OAE minerals, olivine and steel slag, on coastal
742 plankton communities. Both minerals released alkalinity, leading to an elevation in pH_T . However, the addition of steel
743 slag exhibited significantly higher efficiency in elevating alkalinity compared to olivine.

744
745 Approximately 1.9 g L^{-1} of olivine powder were added in the olivine treatments, leading to a $29 \mu\text{mol kg}^{-1}$ increase in
746 alkalinity and increased concentrations of $\text{Si}(\text{OH})_4$ and trace metals (Fe and Ni). Compared to this relatively modest
747 increase of alkalinity and associated CO_2 removal potential, the impacts on the plankton community appeared to be
748 relatively pronounced. Thus, although our experiment ran for only 3 weeks, and olivine powder may slowly release more
749 alkalinity, the short-term response monitored here suggests that the immediate climatic benefit is relatively small compared
750 to a relatively pronounced environmental effect.

751
752 Only 0.038 g L^{-1} of slag were added to the treatment but this led to an alkalinity enhancement of $361 \mu\text{mol kg}^{-1}$ and the
753 increased concentrations of macronutrients (P and Si) and trace metals (Mn and Fe) additions as well as changes in
754 carbonate chemistry. Although limited environmental impacts were observed from the slag treatment in our experiment,
755 some aspects require further study. For example, the pronounced release of P could cause eutrophication and the relatively
756 rapid increase in pH may be a detrimental aspect if organisms cannot acclimate fast enough. Furthermore, it is essential to
757 consider that the composition of steel slag can vary depending on the source factory (Wang et al., 2011; Proctor et al.,
758 2000), which may affect the efficiency of carbon removal and change the trace metal perturbation. Nevertheless, just based
759 on our experiment, the comparison between the immediate climatic benefit and environmental effect appears to be more
760 favourable for slag than olivine.

761

762 Based on our findings, it can be concluded that steel slag powder exhibited fewer environmental impacts on plankton
763 communities compared to olivine powder relative to its capacity for alkalinity enhancement. The results highlight the
764 importance of carefully assessing the environmental consequences of using specific OAE minerals, particularly when
765 considering their potential effects on plankton communities.

766

767 **Data availability.** Data are available in the Institute for Marine and Antarctic Studies (IMAS) data catalogue, University
768 of Tasmania (UTAS) (<https://doi.org/10.25959/X6FH-9K15>, Guo, J., & Bach, L. (2023)).

769

770 **Author contributions.** LTB, RFS, KMS and JAG designed the experiments and JAG carried them out. LTB, RFS and
771 KMS supervised the study. ATT analysed the dissolved/particulate trace metal samples. JAG conducted statistical analyses.
772 JAG prepared the manuscript with contributions from all authors.

773

774 **Competing interests.** The contact author has declared that none of the authors has any competing interests.

775

776 **Disclaimer.** Publisher's note: Copernicus Publications remains neutral with regard to jurisdictional claims in published
777 maps and institutional affiliations.

778

779 **Acknowledgements.** We would like to thank Steve Van Orsouw from Moyne Shire Council, Victoria, Australia for
780 providing olivine rocks. We also thank Bradley Mansell who provided the Basic Oxygen Slag from Liberty Primary Steel
781 Whyalla Steelworks in Whyalla, South Australia, Australia. We thank Sandrin Feig and Thomas Rodemann for their support
782 on scanning electron microscopy and particulate organic matter. We appreciate the assistance of Pam Quayle and Axel
783 Durand (IMAS) in the lab, particularly with particulate metal digestions.

784

785 **Financial support.** This research has been supported by the Australian Research Council through a Future Fellowship
786 project (FT200100846 to LTB), the Carbon to Sea Initiative (LTB), and by the Australian Antarctic Program Partnership
787 (ASCI000002 to RFS, KMS and JAG). Access to SF-ICP-MS instrumentation was facilitated through ARC LIEF funding
788 (LE0989539) awarded to ATT. JAG thanks the Australian Research Training Program (RTP) for her scholarship.

789 References

- 790 Ackerman, L., Jelínek, E., Medaris, G., Ježek, J., Siebel, W., and Strnad, L.: Geochemistry of Fe-rich peridotites and
791 associated pyroxenites from Horní Bory, Bohemian Massif: Insights into subduction-related melt–rock reactions,
792 *Chem. Geol.*, 259, 152-167, <https://doi.org/10.1016/j.chemgeo.2008.10.042>, 2009.
- 793 Al-Azri, A., Al-Hashmi, K., Goes, J., Gomes, H., Rushdi, A. I., Al-Habsi, H., Al-Khusaibi, S., Al-Kindi, R., and Al-Azri, N.:
794 Seasonality of the bloom-forming heterotrophic dinoflagellate *Noctiluca scintillans* in the Gulf of Oman in relation
795 to environmental conditions, *Int. J. Oceans Oceanogr.*, 2, 51-60, 2007.
- 796 Armstrong, F. A.: Why did nature choose manganese to make oxygen?, *Philos Trans R Soc Lond B Biol Sci*, 363, 1263-1270,
797 <https://doi.org/10.1098/rstb.2007.2223>, 2008.
- 798 Bach, L. T., Gill, S. J., Rickaby, R. E. M., Gore, S., and Renforth, P.: CO₂ removal with enhanced weathering and ocean
799 alkalinity enhancement: potential risks and co-benefits for marine pelagic ecosystems, *Front Clim*, 1, 1-21,
800 <http://doi.org/10.3389/fclim.2019.00007>, 2019.
- 801 Balaguer, J., Koch, F., Hassler, C. et al.: Iron and manganese co-limit the growth of two phytoplankton groups dominant at
802 two locations of the Drake Passage. *Commun Biol* 5, 207, <https://doi.org/10.1038/s42003-022-03148-8>, 2022.

803 Baliarsingh, S. K., Lotliker, A. A., Trainer, V. L., Wells, M. L., Parida, C., Sahu, B. K., Srichandan, S., Sahoo, S., Sahu, K. C., and
804 Kumar, T. S.: Environmental dynamics of red *Noctiluca scintillans* bloom in tropical coastal waters, *Mar. Pollut. Bull.*,
805 111, 277-286, <https://doi.org/10.1016/j.marpolbul.2016.06.103>, 2016.

806 Basu, S. and Mackey, K. R. M.: Phytoplankton as key mediators of the biological carbon pump: their responses to a
807 changing climate, *Sustainability*, 10, 869, <https://doi.org/10.3390/su10030869>, 2018.

808 Behrenfeld, M. J., Worthington, K., Sherrell, R. M., Chavez, F. P., Strutton, P., McPhaden, M., and Shea, D. M.: Controls on
809 tropical Pacific Ocean productivity revealed through nutrient stress diagnostics, *Nature*, 442, 1025-1028,
810 <https://doi.org/10.1038/nature05083>, 2006.

811 Bowie, A. R., Townsend, A. T., Lannuzel, D., Remenyi, T. A., and van der Merwe, P.: Modern sampling and analytical
812 methods for the determination of trace elements in marine particulate material using magnetic sector inductively
813 coupled plasma-mass spectrometry, *Anal Chim Acta*, 676, 15-27, <https://doi.org/10.1016/j.aca.2010.07.037>, 2010.

814 Boyd, P. W., Strzepek, R. F., Ellwood, M. J., Hutchins, D. A., Nodder, S. D., Twining, B. S., and Wilhelm, S. W.: Why are biotic
815 iron pools uniform across high- and low-iron pelagic ecosystems?, *Global Biogeochem. Cycles*, 29, 1028-1043,
816 <http://doi.org/10.1002/2014gb005014>, 2015.

817 Boyd, P. W., Jickells, T., Law, C., Blain, S., Boyle, E., Buesseler, K., Coale, K., Cullen, J., De Baar, H. J., and Follows, M.:
818 Mesoscale iron enrichment experiments 1993-2005: synthesis and future directions, *Science*, 315, 612-617,
819 <http://doi.org/10.1126/science.1131669>, 2007.

820 Bruland, K. W. and Lohan, M. C.: 6.02 Controls of Trace Metals in Seawater, in: *Treatise on Geochemistry*, edited by:
821 Elderfield, H., Holland, H. D., and Turekian, K. K., Elsevier Pergamon, 23-47, [http://doi.org/10.1016/b0-08-043751-](http://doi.org/10.1016/b0-08-043751-6/06105-3)
822 [6/06105-3](http://doi.org/10.1016/b0-08-043751-6/06105-3), 2003.

823 Burt, D. J., Fröb, F., and Ilyina, T.: The sensitivity of the marine carbonate system to regional ocean alkalinity enhancement,
824 *Front Clim*, 3, <http://doi.org/10.3389/fclim.2021.624075>, 2021.

825 Caserini, S., Storni, N., and Grosso, M.: The availability of limestone and other raw materials for ocean alkalinity
826 enhancement, *Global Biogeochem. Cycles*, 36, <http://doi.org/10.1029/2021gb007246>, 2022.

827 De Baar, H. J., Boyd, P. W., Coale, K. H., Landry, M. R., Tsuda, A., Assmy, P., Bakker, D. C., Bozec, Y., Barber, R. T., and Brzezinski,
828 M. A.: Synthesis of iron fertilization experiments: from the iron age in the age of enlightenment, *J Geophys Res*
829 *Oceans*, 110, <https://doi.org/10.1029/2004JC002601>, 2005.

830 Dickson, A. G., Sabine, C. L., and Christian, J. R.: *Guide to best practices for ocean CO₂ measurements*, North Pacific Marine
831 Science Organization, Canada2007.

832 Egge, J. and Jacobsen, A.: Influence of silicate on particulate carbon production in phytoplankton, *Mar. Ecol. Prog. Ser.*,
833 147, 219-230, <http://doi.org/10.3354/meps147219>, 1997.

834 Evans, C., O'Reilly, J. E., and Thomas, J.: *A handbook for the measurement of chlorophyll and primary production*, 1987.

835 Falkowski, P. G.: The role of phytoplankton photosynthesis in global biogeochemical cycles, *Photosynthesis Research*, 39,
836 235-258, <https://doi.org/10.1007/BF00014586>, 1994.

837 Feng, E. Y., Koeve, W., Keller, D. P., and Oschlies, A.: Model-based assessment of the CO₂ sequestration potential of coastal
838 ocean alkalization, *Earth's Future*, 5, 1252-1266, <http://doi.org/10.1002/2017ef000659>, 2017.

839 Ferderer, A., Chase, Z., Kennedy, F., Schulz, K. G., and Bach, L. T.: Assessing the influence of ocean alkalinity enhancement
840 on a coastal phytoplankton community, *Biogeosciences*, 19, 5375-5399, <http://doi.org/10.5194/bg-19-5375-2022>,
841 2022.

842 Ferderer, A., Schulz, K. G., Riebesell, U., Baker, K. G., Chase, Z., and Bach, L. T.: Investigating the effect of silicate and calcium
843 based ocean alkalinity enhancement on diatom silicification, *Biogeosciences Discuss.* [preprint],
844 <https://doi.org/10.5194/bg-2023-144>, in review, 2023.

845 Package 'seacarb'-Seawater Carbonate Chemistry: <https://cran.r-project.org/web/packages/seacarb/index.html>, last
846 access: 2023/6/1.

847 Gaulier, C., Zhou, C., Guo, W., Bratkic, A., Supervielle, P. J., Billon, G., Baeyens, W., and Gao, Y.: Trace metal speciation in
848 North Sea coastal waters, *Sci. Total Environ.*, 692, 701-712, <http://doi.org/10.1016/j.scitotenv.2019.07.314>, 2019.

849 Guo, J., Bao, Y., and Wang, M.: Steel slag in China: Treatment, recycling, and management, *Waste Management*, 78, 318-
850 330, <https://doi.org/10.1016/j.wasman.2018.04.045>, 2018.

851 Guo, J. A., Strzepek, R., Willis, A., Ferderer, A., and Bach, L. T.: Investigating the effect of nickel concentration on
852 phytoplankton growth to assess potential side-effects of ocean alkalinity enhancement, *Biogeosciences*, 19, 3683-
853 3697, <https://doi.org/10.5194/bg-19-3683-2022>, 2022.

854 Hallegraeff, G. M., Albinsson, M. E., Dowdney, J., Holmes, A. K., Mansour, M. P., and Seger, A.: Prey preference,
855 environmental tolerances and ichthyotoxicity by the red-tide dinoflagellate *Noctiluca scintillans* cultured from
856 Tasmanian waters, *J. Plankton Res.*, 41, 407-418, <https://doi.org/10.1093/plankt/fbz037>, 2019.

857 Hansen, H. P. and Koroleff, F.: Determination of nutrients, in: *Methods of seawater analysis*, edited by: Grasshoff, K.,
858 Kremling, K., and Ehrhardt, M., 159-228, <https://doi.org/10.1002/9783527613984.ch10>, 1999.

859 Hartmann, J., West, A. J., Renforth, P., Köhler, P., De La Rocha, C. L., Wolf-Gladrow, D. A., Dürr, H. H., and Scheffran, J.:

860 Enhanced chemical weathering as a geoengineering strategy to reduce atmospheric carbon dioxide, supply
861 nutrients, and mitigate ocean acidification, *Rev. Geophys.*, 51, 113-149, <http://doi.org/10.1002/rog.20004>, 2013.

862 Humphreys, M. P., Lewis, E. R., Sharp, J. D., and Pierrot, D.: PyCO2SYS v1. 8: marine carbonate system calculations in
863 Python, *Geosci Model Dev*, 15, 15-43, <https://doi.org/10.5194/gmd-15-15-2022>, 2022.

864 Hutchins, D. A., Fu, F.-X., Yang, S.-C., John, S. G., Romaniello, S. J., Andrews, M. G., and Walworth, N. G.: Responses of
865 globally important phytoplankton species to olivine dissolution products and implications for carbon dioxide
866 removal via ocean alkalinity enhancement, *Biogeosciences*, 20, 4669–4682, [https://doi.org/10.5194/bg-20-4669-](https://doi.org/10.5194/bg-20-4669-2023)
867 2023, 2023.

868 Ilyina, T., Wolf-Gladrow, D., Munhoven, G., and Heinze, C.: Assessing the potential of calcium-based artificial ocean
869 alkalization to mitigate rising atmospheric CO2 and ocean acidification, *Geophys. Res. Lett.*, 40, 5909-5914,
870 <https://doi.org/10.1002/2013GL057981>, 2013.

871 Jakimska, A., Konieczka, P., Skóra, K., and Namieśnik, J.: Bioaccumulation of metals in tissues of marine animals, Part II:
872 metal concentrations in animal tissues, *Pol J Environ Stud*, 20, 2011.

873 Keller, D. P., Feng, E. Y., and Oschlies, A.: Potential climate engineering effectiveness and side effects during a high carbon
874 dioxide-emission scenario, *Nat. Commun.*, 5, 3304, <https://doi.org/10.1038/ncomms4304>, 2014.

875 King, A. L., Sañudo-Wilhelmy, S. A., Boyd, P. W., Twining, B. S., Wilhelm, S. W., Breebe, C., Ellwood, M. J., and Hutchins, D.
876 A.: A comparison of biogenic iron quotas during a diatom spring bloom using multiple approaches, *Biogeosciences*,
877 9, 667-687, <http://doi.org/10.5194/bg-9-667-2012>, 2012.

878 Kohler, P., Hartmann, J., and Wolf-Gladrow, D. A.: Geoengineering potential of artificially enhanced silicate weathering of
879 olivine, *Proc. Natl. Acad. Sci. USA*, 107, 20228-20233, <https://doi.org/10.1073/pnas.1000545107>, 2010.

880 Kourounis, S., Tsvilis, S., Tsakiridis, P. E., Papadimitriou, G. D., and Tsiabouki, Z.: Properties and hydration of blended
881 cements with steelmaking slag, *Cem. Concr. Res.*, 37, 815-822, <https://doi.org/10.1016/j.cemconres.2007.03.008>,
882 2007.

883 Kulkarni, P. P., She, Y. M., Smith, S. D., Roberts, E. A., and Sarkar, B.: Proteomics of metal transport and metal-associated
884 diseases, *Chemistry*, 12, 2410-2422, <http://doi.org/10.1002/chem.200500664>, 2006.

885 Lenton, A., Matear, R. J., Keller, D. P., Scott, V., and Vaughan, N. E.: Assessing carbon dioxide removal through global and
886 regional ocean alkalization under high and low emission pathways, *Earth. Syst. Dyn.*, 9, 339-357,
887 <https://doi.org/10.5194/esd-9-339-2018>, 2018.

888 Lombard, F., Selander, E., and Kjørboe, T.: Active prey rejection in the filter-feeding appendicularian *Oikopleura dioica*,
889 *Limnol. Oceanogr.*, 56, 1504-1512, <http://doi.org/10.4319/lo.2011.56.4.1504>, 2011.

890 Lueker, T. J., Dickson, A. G., and Keeling, C. D.: Ocean pCO2 calculated from dissolved inorganic carbon, alkalinity, and
891 equations for K1 and K2: validation based on laboratory measurements of CO2 in gas and seawater at equilibrium,
892 *Mar. Chem.*, 70, 105-119, [https://doi.org/10.1016/S0304-4203\(00\)00022-0](https://doi.org/10.1016/S0304-4203(00)00022-0), 2000.

893 Macleod, C. and Coughanowr, C.: Heavy metal pollution in the Derwent estuary: History, science and management, *Reg.*
894 *Stud. Mar. Sci.*, 32, <http://doi.org/10.1016/j.rsma.2019.100866>, 2019.

895 Moore, C. M., Mills, M. M., Arrigo, K. R., Berman-Frank, I., Bopp, L., Boyd, P. W., Galbraith, E. D., Geider, R. J., Guieu, C.,
896 Jaccard, S. L., Jickells, T. D., La Roche, J., Lenton, T. M., Mahowald, N. M., Marañón, E., Marinov, I., Moore, J. K.,
897 Nakatsuka, T., Oschlies, A., Saito, M. A., Thingstad, T. F., Tsuda, A., and Ulloa, O.: Processes and patterns of oceanic
898 nutrient limitation, *Nat. Geosci.*, 6, 701-710, <http://doi.org/10.1038/ngeo1765>, 2013.

899 Nelson, D. M., Smith Jr, W. O., Muench, R. D., Gordon, L. I., Sullivan, C. W., and Husby, D. M.: Particulate matter and nutrient
900 distributions in the ice-edge zone of the Weddell Sea: relationship to hydrography during late summer, *Deep. Sea.*
901 *Res. A*, 36, 191-209, [https://doi.org/10.1016/0198-0149\(89\)90133-7](https://doi.org/10.1016/0198-0149(89)90133-7), 1989.

902 NRMCM, N. a.: The Australian Drinking Water Guidelines (2011) - Version 3.8 Updated 2022, 2022.

903 Pausch, F., Bischof, K., Trimborn, S.: Iron and manganese co-limit growth of the Southern Ocean diatom *Chaetoceros debilis*.
904 *PLOS ONE* 14, e0221959. <https://doi.org/10.1371/journal.pone.0221959>, 2019.

905 Paquay, F. S. and Zeebe, R. E.: Assessing possible consequences of ocean liming on ocean pH, atmospheric CO2
906 concentration and associated costs, *Int. J. Greenh. Gas Control.*, 17, 183-188,
907 <https://doi.org/10.1016/j.ijggc.2013.05.005>, 2013.

908 Platt, T., Gallegos, C. L., and Harrison, W. G.: Photoinhibition of photosynthesis in natural assemblages of marine
909 phytoplankton, *J. Mar. Res.*, 38, 687-701, 1980.

910 Proctor, D. M., Fehling, K. A., Shay, E. C., Wittenborn, J. L., Green, J. J., Avent, C., Bigham, R. D., Connolly, M., Lee, B.,
911 Shepker, T. O., and Zak, M. A.: Physical and chemical characteristics of blast furnace, basic oxygen furnace, and
912 electric arc furnace steel industry slags, *Environ. Sci. Technol.*, 34, 1576-1582, <http://doi.org/10.1021/es9906002>,
913 2000.

914 Reichl, C., Schatz, M., and Zsak, G.: World mining data, 1-261, 2018.

915 Renforth, P.: The negative emission potential of alkaline materials, *Nat. Commun.*, 10, [http://doi.org/10.1038/s41467-](http://doi.org/10.1038/s41467-019-09475-5)
916 019-09475-5, 2019.

917 Renforth, P. and Henderson, G.: Assessing ocean alkalinity for carbon sequestration, *Rev. Geophys.*, 55, 636-674,
918 <http://doi.org/10.1002/2016rg000533>, 2017.

919 Schallenberg, C., Strzepek, R. F., Schuback, N., Clementson, L. A., Boyd, P. W., and Trull, T. W.: Diel quenching of Southern
920 Ocean phytoplankton fluorescence is related to iron limitation, *Biogeosciences*, 17, 793-812,
921 <https://doi.org/10.5194/bg-17-793-2020>.

922 Schuiling, R. D. and Krijgsman, P.: Enhanced weathering: an effective and cheap tool to sequester CO₂, *Clim. Change*, 74,
923 349-354, <https://doi.org/10.1007/s10584-005-3485-y>, 2006.

924 Selfe, C.: Developing Transfer Function to Measuring Phytoplankton Cellular Properties with Flow Cytometry, Master's
925 thesis, Institute of Marine and Antarctic Studies, University of Tasmania, Australia, 2022.

926 Comparing smooths in factor-smooth interactions II ordered factors:
927 <https://fromthebottomoftheheap.net/2017/12/14/difference-splines-ii/>, last access: March 2023.

928 Smith, S. M., Geden, O., Nemet, G. F., Gidden, M. J., Lamb, W. F., Powis, C., Bellamy, R., Callaghan, M. W., Cowie, A., Cox,
929 E., Fuss, S., Gasser, T., Grassi, G., Greene, J., Lück, S., Mohan, A., Müller-Hansen, F., Peters, G. P., Pratama, Y., Repke,
930 T., Riahi, K., Schenuit, F., Steinhäuser, J., Streifer, J., Valenzuela, J. M., and Minx, J. C.: The State of Carbon Dioxide
931 Removal - 1st Edition, <http://doi.org/10.17605/OSF.IO/W3B4Z>, 2023.

932 Sohrin, Y. and Bruland, K. W.: Global status of trace elements in the ocean, *TrAC, Trends Anal. Chem.*, 30, 1291-1307,
933 <https://doi.org/10.1016/j.trac.2011.03.006>, 2011.

934 Strzepek, R. F. and Harrison, P. J.: Photosynthetic architecture differs in coastal and oceanic diatoms, *Nature*, 431, 689-
935 692, <http://doi.org/10.1038/nature02954>, 2004.

936 Su, B., Chen, Y., Guo, S., and Liu, J.: Origins of orogenic dunites: petrology, geochemistry, and implications, *Gondwana Res.*,
937 29, 41-59, <https://doi.org/10.1016/j.gr.2015.08.001>, 2016.

938 Subhas, A. V., Marx, L., Reynolds, S., Flohr, A., Mawji, E. W., Brown, P. J., and Cael, B.: Microbial ecosystem responses to
939 alkalinity enhancement in the North Atlantic Subtropical Gyre, *Front Clim*, 4,
940 <https://doi.org/10.3389/fclim.2022.784997>, 2022.

941 Sunda, W. G.: Trace metal-phytoplankton interactions in aquatic systems, in: *Environmental Microbe-Metal Interactions*,
942 edited by: Lovley, D. R., 79-107, <https://doi.org/10.1128/9781555818098.ch4>, 2000.

943 Sunda, W. G.: Feedback interactions between trace metal nutrients and phytoplankton in the ocean, *Frontiers in*
944 *Microbiology*, 3, 1-22, <http://doi.org/10.3389/fmicb.2012.00204>, 2012.

945 Sunda, W. G. and Huntsman, S. A.: Iron Uptake and Growth Limitation in Oceanic and Coastal Phytoplankton, *Marine*
946 *Chemistry*, 50, 189-206, Doi 10.1016/0304-4203(95)00035-P, 1995.

947 Sunda, W. G. and Huntsman, S. A.: Interrelated influence of iron, light and cell size on marine phytoplankton growth,
948 *Nature*, 390, 389-392, <http://doi.org/10.1038/37093>, 1997.

949 Tang, D. G. and Morel, F. M. M.: Distinguishing between cellular and Fe-oxide-associated trace elements in phytoplankton,
950 *Mar. Chem.*, 98, 18-30, <http://doi.org/10.1016/j.marchem.2005.06.003>, 2006.

951 Tovar-Sanchez, A., Sanudo-Wilhelmy, S. A., Garcia-Vargas M., Weaver R. S., Popels L., C., and Hutchins D. A.: A trace metal
952 clean reagent to remove surface-bound iron from marine phytoplankton. *Mar. Chem.*, 82, 1-2, 91-99,
953 [https://doi.org/10.1016/S0304-4203\(03\)00054-9](https://doi.org/10.1016/S0304-4203(03)00054-9), 2003.

954 Twining, B. S. and Baines, S. B.: The trace metal composition of marine phytoplankton, *Ann. Rev. Mar. Sci.*, 5, 191-215,
955 <http://doi.org/10.1146/annurev-marine-121211-172322>, 2013.

956 Wafar, M., Le Corre, P., and L'Helguen, S.: f-Ratios calculated with and without urea uptake in nitrogen uptake by
957 phytoplankton, *Deep Sea Res. I Oceanogr. Res. Pap.*, 42, 1669-1674, [https://doi.org/10.1016/0967-0637\(95\)00066-F](https://doi.org/10.1016/0967-0637(95)00066-F), 1995.

959 Wang, Q., Yan, P., and Feng, J.: A discussion on improving hydration activity of steel slag by altering its mineral
960 compositions, *J. Hazard. Mater.*, 186, 1070-1075, <https://doi.org/10.1016/j.jhazmat.2010.11.109>, 2011.

961 Wang, W.: Interactions of trace metals and different marine food chains, *Mar. Ecol. Prog. Ser.*, 243, 295-309,
962 <http://doi.org/10.3354/meps243295>, 2002.

963 Wolfe-Simon, F., Grzebyk, D., Schofield, O., and Falkowski, P. G.: The role and evolution of superoxide dismutases in algae,
964 *J. Phycol.*, 41, 453-465, <https://doi.org/10.1111/j.1529-8817.2005.00086.x>, 2005.

965 Xin, X., Faucher, G., and Riebesell, U.: Phytoplankton response to Increased nickel in the context of ocean alkalinity
966 enhancement, *Biogeosciences* [preprint], <https://doi.org/10.5194/bg-2023-130>, 2023.

967 Zhang, W., Dong, Z., Zhang, C., Sun, X., Hou, C., Liu, Y., Wang, L., Ma, Y., and Zhao, J.: Effects of physical-biochemical
968 coupling processes on the *Noctiluca scintillans* and *Mesodinium* red tides in October 2019 in the Yantai nearshore,
969 China, *Mar. Pollut. Bull.*, 160, 111609, <https://doi.org/10.1016/j.marpolbul.2020.111609>, 2020.

970